J Neurophysiol 119: 2358–2372, 2018.
First published March 21, 2018; doi:10.1152/jn.00867.2017.

RESEARCH ARTICLE | *Cellular and Molecular Properties of Neurons*

Inward rectifier potassium current I_{Kir} promotes intrinsic pacemaker activity of thalamocortical neurons

Yimy Amarillo,[1,3] Angela I. Tissone,[1,3,4] Germán Mato,[2,3] and Marcela S. Nadal[1,3,4]

[1]*Departamento de Física Médica, Centro Atómico Bariloche and Instituto Balseiro, Consejo Nacional de Investigaciones Científicas y Técnicas (CONICET), San Carlos de Bariloche, Río Negro, Argentina;* [2]*Departamento de Física Médica, Centro Atómico Bariloche and Instituto Balseiro, Comisión Nacional de Energía Atómica (CNEA), Consejo Nacional de Investigaciones Científicas y Técnicas (CONICET), San Carlos de Bariloche, Río Negro, Argentina;* [3]*Gerencia de Área Investigación y Aplicaciones no Nucleares, Gerencia de Física, Departamento Sistemas Complejos y Altas Energías, División Física Estadística e Interdisciplinaria, Centro Atómico Bariloche, San Carlos de Bariloche, Río Negro, Argentina; and* [4]*Universidad Nacional del Comahue, Centro Regional Universitario Bariloche, San Carlos de Bariloche, Río Negro, Argentina*

Submitted 6 December 2017; accepted in final form 16 March 2018

Amarillo Y, Tissone AI, Mato G, Nadal MS. Inward rectifier potassium current I_{Kir} promotes intrinsic pacemaker activity of thalamocortical neurons. *J Neurophysiol* 119: 2358–2372, 2018. First published March 21, 2018; doi:10.1152/jn.00867.2017.—Slow repetitive burst firing by hyperpolarized thalamocortical (TC) neurons correlates with global slow rhythms (<4 Hz), which are the physiological oscillations during non-rapid eye movement sleep or pathological oscillations during idiopathic epilepsy. The pacemaker activity of TC neurons depends on the expression of several subthreshold conductances, which are modulated in a behaviorally dependent manner. Here we show that upregulation of the small and neglected inward rectifier potassium current I_{Kir} induces repetitive burst firing at slow and delta frequency bands. We demonstrate this in mouse TC neurons in brain slices by manipulating the Kir maximum conductance with dynamic clamp. We also performed a thorough theoretical analysis that explains how the unique properties of I_{Kir} enable this current to induce slow periodic bursting in TC neurons. We describe a new ionic mechanism based on the voltage- and time-dependent interaction of I_{Kir} and hyperpolarization-activated cationic current I_h that endows TC neurons with the ability to oscillate spontaneously at very low frequencies, even below 0.5 Hz. Bifurcation analysis of conductance-based models of increasing complexity demonstrates that I_{Kir} induces bistability of the membrane potential at the same time that it induces sustained oscillations in combination with I_h and increases the robustness of low threshold-activated calcium current I_T-mediated oscillations.

NEW & NOTEWORTHY The strong inwardly rectifying potassium current I_{Kir} of thalamocortical neurons displays a region of negative slope conductance in the current-voltage relationship that generates potassium currents activated by hyperpolarization. Bifurcation analysis shows that I_{Kir} induces bistability of the membrane potential; generates sustained subthreshold oscillations by interacting with the hyperpolarization-activated cationic current I_h; and increases the robustness of oscillations mediated by the low threshold-activated calcium current I_T. Upregulation of I_{Kir} in thalamocortical neurons induces repetitive burst firing at slow and delta frequency bands (<4 Hz).

Kir channels; repetitive burst firing; subthreshold conductances; thalamocortical neurons

INTRODUCTION

Generation and maintenance of global brain rhythms in the slow and delta bands (<4 Hz) that characterize non-rapid eye movement (NREM) sleep and idiopathic epilepsies are associated with the intrinsic oscillatory behavior of thalamocortical (TC) neurons in the thalamus (Curró-Dossi et al. 1992; McCormick and Pape 1990b; Soltesz et al. 1991; Steriade and Contreras 1995). Depending on the level of their resting membrane potential, these neurons display two firing modes that correlate with distinct behavioral states. During the waking, alert states, TC neurons are depolarized and fire action potentials tonically at variable frequencies (Steriade et al. 1996), which are synchronized over specific thalamocortical circuits (Buzsáki 2006). In contrast, a large-scale synchronization of sustained, low-frequency oscillations characterizes unconscious states like slow-wave sleep (Steriade 1997) and absence seizures (Steriade and Contreras 1995). The slow rhythms (<4 Hz) that characterize these physiological and pathological states are correlated with repetitive burst firing by hyperpolarized TC neurons (Steriade and Contreras 1995). At subthreshold membrane potentials, TC neurons fire repetitive bursts of action potentials thanks to a unique set of ion conductances, including the essential calcium current I_T that generates low-threshold spikes (LTSs) (Amarillo et al. 2014). Electrophysiological studies on genetically modified animals also link the mechanisms that control the subthreshold excitability and the repetitive burst firing of TC neurons with the expression of sleep rhythms and epileptic oscillations. For example, there is a large decrease of delta oscillations during NREM sleep in mice that lack the ion channel subunit ($Ca_v3.1$) responsible for the low-threshold calcium current I_T (Lee et al.

Address for reprint requests and other correspondence: Y. Amarillo, Consejo Nacional de Investigaciones Científicas y Técnicas, Departamento de Física Médica, Centro Atómico Bariloche, Avenida Bustillo 9500, San Carlos de Bariloche, Rio Negro, Argentina (e-mail: amarillo@cab.cnea.gov.ar).

2004), which is essential for the intrinsic oscillations in TC neurons. On the other hand, either overexpression of I_T or elimination of the hyperpolarization-activated cationic current I_h—another important current that controls the excitability of TC neurons (Amarillo et al. 2014, 2015)—results in a phenotype of absence epilepsy characterized by spike and wave discharges at ~3 Hz (Ernst et al. 2009; Ludwig et al. 2003).

From a theoretical point of view, the minimal requirements to generate membrane potential oscillations are the combination of an amplifying variable and a resonant variable in the presence of leak conductances (Hutcheon and Yarom 2000; Izhikevich 2005). The biophysical properties of the T-type calcium channels allow for spontaneous, subthreshold oscillations, since I_T behaves as both an amplifying current (through the activation gate m_T) and a resonant current (through the inactivation gate h_T) (Amarillo et al. 2015). The bifurcation analysis of the minimal I_T-Leaks model of TC neurons uncovered the dynamic interplay of these two variables in the generation and maintenance of intrinsic oscillations in the delta band (Amarillo et al. 2015).

Besides I_T and the potassium and sodium leak currents, another four subthreshold conductances modulate and control the propensity of TC neurons to oscillate at low frequencies (Amarillo et al. 2014). The interaction of the voltage- and time-dependent properties of these seven ion channels establishes the sequence of events that underlie the generation and maintenance of repetitive burst firing in TC neurons (Amarillo et al. 2014). We demonstrated that I_h has a stabilizing role in the oscillations, since it amplifies the range of membrane voltage at which the oscillations can occur (Amarillo et al. 2015). Our analysis also suggested that the inward rectifier potassium current I_{Kir} (largely mediated by Kir2.2 channels in TC neurons; Amarillo et al. 2014) promotes the periodicity of I_T- mediated burst firing by potentiating interburst hyperpolarizations (Amarillo et al. 2014). I_{Kir} behaves as a hyperpolarization-activated outward current because of the existence of a negative slope region in the current-voltage (*I/V*) relationship. In this negative slope conductance region, displacements of the membrane potential in the hyperpolarizing direction produce the regenerative activation (unblock) of I_{Kir} and thereby regenerative hyperpolarization. Progressive hyperpolarization removes inactivation of I_T at the same time that it induces activation of I_h, which brings the membrane potential back to the region of activation of I_T. Here we show that an increase (introduced with dynamic clamp) in Kir maximum conductance in TC neurons recorded from mouse brain slices elicits oscillations at delta and slow frequencies in all the recorded neurons. This suggests that upregulation of I_{Kir} in TC neurons could amplify the natural resonance of TC neurons at burst firing frequencies, thereby increasing the propensity of the thalamocortical system to synchronize at these slow frequencies. This mechanism could take place physiologically during NREM sleep or pathologically during epilepsy.

METHODS

Computational modeling. For this study, we used Hodgkin and Huxley-like equations similar to those used previously (Amarillo et al. 2014). Bifurcation analysis and phase-plane portrait analysis were performed with XPPAUT (Ermentrout 2002), using absolute values of maximum conductance or permeability (in nS or cm^3/s, respectively). Time course simulations were performed with the NEURON environment (Hines and Carnevale 1997), where per-unit area values were used (in S/cm^2 or cm/s, respectively). The interconversion between absolute and per-unit area values was carried out considering a total capacitance of 0.2 nF for all model cells. In Table 1 we report the absolute values. Time course simulations were performed assuming a temperature of 28°C (to match the temperature of the in vitro recordings), and the equations of time dependence (time constants) were adjusted accordingly by using the reported Q_{10} conversion factors (Table 1).

The voltage equations have the form

$$dV/dt = \left(I_{inj} - \Sigma I_i\right)/C \quad (1)$$

where I_{inj} is the magnitude of injected current, C is the capacitance, and ΣI_i is the sum of all ionic currents as follows: $\Sigma I_i = I_{Kir} + I_{Kleak} + I_{Naleak}$ for the minimal I_{Kir}-Leaks model; $\Sigma I_i = I_{Kir} + I_h + I_{Kleak} + I_{Naleak}$ for the minimal I_{Kir}-I_h-Leaks model; $\Sigma I_i = I_{Kir} + I_h + I_T + I_{Kleak} + I_{Naleak}$ for the I_{Kir}-I_h-I_T-Leaks model; and $\Sigma I_i = I_{Kir} + I_h + I_T + I_A + I_{NaP} + I_{Na} + I_K + I_L + I_{AHP} + I_{KCa} + I_{CAN} + I_{Kleak} + I_{Naleak}$ for the more complete model that includes subthreshold and suprathreshold operating conductances.

The current equations for all ionic currents, except the calcium currents I_T and I_L, have the form

$$I_i = \bar{g}_i m_i^p(V,t) h_i^q(V,t)\left(V - E_i\right) \quad (2)$$

where I_i is a given ionic current; $\bar{g}_i$ is the maximum conductance for current i; m_i and h_i are the voltage- and time-dependent activation and inactivation variables for that current respectively; p and q are exponents; V is voltage, and E_i is the reversal potential for that current. Activation of currents I_{Kir}, I_{NaP}, I_{AHP}, and I_{KCa} was assumed to be instantaneous; therefore, for these currents the time-dependent $m_i^p(V,t)$ variable was replaced by $m_{j\infty}^p(V)$ in *Eq. 2*.

To eliminate the negative slope conductance region in the simulated steady-state *I/V* relationship of I_{Kir} (Fig. 4*A*), we modified the original Boltzmann equation that was obtained by fitting experimental data (Table 1) and replaced it by

$$m_\infty = 0.9/\left\{1 + \exp\left[\left(V + 97.9\right)/9.7\right]\right\} + 0.1 \quad (3)$$

Current equations for the calcium currents are

$$I_i = p_i m_i^p h_T^q G\left(V, Ca_o, Ca_i\right) \quad (4)$$

where p_i is the maximum permeability, m_i and h_i are the activation and inactivation variables, respectively, and $G(V, Ca_o, Ca_i)$ is the nonlinear Goldman-Hodgkin-Katz function of potential and calcium concentration:

$$G\left(V, Ca_o, Ca_i\right) = z^2F^2V/RT\left(Ca_i - Ca_o\exp\left[-zFV/RT\right]\right) / \left(1 - \exp\left[-zFV/RT\right]\right) \quad (5)$$

where Ca_o and Ca_i are the extracellular and the intracellular concentrations of Ca^{2+} and z, F, R, and T are the valence, Faraday constant, gas constant, and absolute temperature, respectively. This constant-field equation is used because of the large ratio between intra- and extracellular calcium concentrations and also because of the nonlinear and far-from-equilibrium behavior of calcium currents (Hille 2001).

The Goldman-Hodgkin-Katz formalism is not suitable to implement artificial I_T with dynamic clamp because it is not possible to control calcium concentrations. Hence, for the experiment with artificial I_T introduced by dynamic clamp, the current equation for I_T (Table 1) was replaced by a Nernstian equation as previously implemented (Hughes et al. 2009):

$$I_T = \bar{g}_T m_T^2 h_T\left(V - E_T\right) \quad (6)$$

where $\bar{g}_T$ is the maximum conductance for I_T and E_T is the reversal potential for calcium (E_T = 130 mV).

Equations for the activation and inactivation variables have the form

Table 1. *Ion channel kinetics and parameters*

I_i	$m_{\infty i}$	$h_{\infty i}$	τ_{mi}	τ_{hi}	p	q	$\bar{g}_i$, nS	E_i, mV
I_{Kir}	$1/\{1 + \exp[(V + 97.9)/9.7]\}$				1	0	30.6	−100
$I_{KirNoNS}$	$0.9/\{1 + \exp[(V + 97.9)/9.7]\} + 0.1$				1	0	30.6	−100
I_{Kleak}					0	0	2.27	−100
I_{Naleak}					0	0	0.68	0
I_T	$1/\{1 + \exp[(V + 53)/-6.2]\}$	$1/\{1 + \exp[(V + 75)/4]\}$	$(0.612 + 1/\{\exp[(V + 128)/-16.7] + \exp[(V + 12.8)/18.2]\})/1.44$	$\{\exp[(V + 461)/66.6]\}/3$ for $V < -75$ $\{28 + \exp[(V + 16)/-10.5]\}/1.44$ for $V > -75$	2	1	9.1*	
I_h	$1/\{1 + \exp[(V + 82)/5.49]\}$		$\{1/[0.0008 + 0.0000035 \exp(-0.05787V) + \exp(-1.87 + 0.0701\ V)]\}/0.43$		1	0	1.82	−43
I_A	$m_{\infty A}1 = 1/\{1 + \exp[-(V + 60)/8.5]\}$ $m_{\infty A}2 = 1/\{1 + \exp[-(V + 36)/20]\}$	$1/\{1 + \exp[(V + 78)/6]\}$	$(0.37 + 1/\{\exp[(V + 35.8)/19.7] + \exp[-(V + 79.7)/12.7]\})/1.67$	$\tau_{hA}1 = (1/\{\exp[(V + 46)/5] + \exp[(-V + 238)/37.5]\})/1.67$ for $V < -63$ $\tau_{hA}1 = 0.735$ for $V > -63$ $\tau_{hA}2 = (1/\{\exp[(V + 46)/5] + \exp[(-V + 238)/37.5]\})/1.67$ for $V < -73$ $\tau_{hA}2 = 44.12$ for $V > -73$	4	1	1,248.5	−100
I_{NaP}	$1/\{1 + \exp[-(V + 57.9)/6.4]\}$	$1/\{1 + \exp[(V + 58.7)/14.2]\}$		$[1{,}000 + (10{,}000/\{1 + \exp[(V + 60)/10]\})]/1.73$	1	1	1.25	+45
I_{Na}	$\alpha_m/(\alpha_m + \beta_m)$ $\alpha_m = 0.32(-V - 37)/\{\exp[(-V - 37)/4] - 1\}$ $\beta_m = 0.28(V + 10)/\{\exp[(V + 10)/5] - 1\}$	$\alpha_h/(\alpha_h + \beta_h)$ $\alpha_h = 0.128\exp[(-V - 33)/18]$ $\beta_h = 4/\{1 + \exp[(-V - 10)/5]\}$	$[1/(\alpha_m + \beta_m)]/0.41$ $\alpha_m = 0.32(-V - 37)/\{\exp[(-V - 37)/4] - 1\}$ $\beta_m = 0.28(V + 10)/\{\exp[(V + 10)/5] - 1\}$	$[1/(\alpha_h + \beta_h)]/0.41$ $\alpha_h = 0.128\exp[(-V - 33)/18]$ $\beta_h = 4/\{1 + \exp[(-V - 10)/5]\}$	3	1	1,135	+45
I_K	$\alpha_m/(\alpha_m + \beta_m)$ $\alpha_m = 0.032(-V - 35)/\{\exp[(-V - 35)/5] - 1\}$ $\beta_m = 0.5\exp[(-V - 40)/40]$		$[1/(\alpha_m + \beta_m)]/0.41$ $\alpha_m = 0.032(-V - 35)/\{\exp[(-V - 35)/5] - 1\}$ $\beta_m = 0.5\exp[(-V - 40)/40]$		4	0	1,135	−100
I_L	$1/\{1 + \exp[(V + 10)/-10]\}$		$[1/(\alpha_m + \beta_m)]/1.32$ $\alpha_m = 1.6/\{1 + \exp[-0.072(V - 5)]\}$ $\beta_m = 0.02(V - 1.31)/\{\exp[(V - 1.31)/5.36] - 1\}$		2	0	9.1*	
I_{AHP}	$\alpha_m/(\alpha_m + \beta_m)$ $\alpha_m = Ca_{iL}/10{,}000$ for $Ca_{iL} < 0.0001$ $\alpha_m = 0.01$ for $Ca_{iL} > 0.0001$ $\beta_m = 0.01$				1	0	1.14	−100
I_{KCa}	$\alpha_m/(\alpha_m + \beta_m)$ $\alpha_m = 2/37.95\{\exp[(V + 50)/11 - (V + 53.5)/27]\}$ for $V < -10$ $\alpha_m = 2\exp[(-V - 53.5)/27]$ for $V > -10$ $\beta_m = 2\exp[(-V - 53.5)/27] - \alpha_m$ for $V < -10$ $\beta_m = 0$ for $V > -10$				1	0	11.35	−100
I_{CAN}	$\alpha_m/(\alpha_m + \beta_m)$ $\alpha_m = 0.0004(Ca_{iT}/0.0001)^8$ $\beta_m = 0.0004$		$[1/(\alpha_m + \beta_m)]/1.93$ for $\tau_{mCAN} \geq 0.1$ 0.1 for $\tau_{mCAN} < 0.1$ $\alpha_m = 0.0004(Ca_{iT}/0.0001)^8$ $\beta_m = 0.0004$		2	0	2.27	−15

As in the original description by Huguenard et al. (1991), I_A is modeled as the sum of 2 currents. The current expression for I_A is $I_A = \bar{g}_A(0.6h_A1m_A1^4 + 0.4\ h_A2m_A2^4)\ (V - E_A)$. As for I_{AHP}, I_{KCa} is gated by changes in the internal concentration of Ca^{2+} that depend on I_L (Ca_{iL}, see METHODS). Thus the current equation of I_{KCa} reflecting this Ca^{2+} dependence is $I_{KCa} = 0.004\bar{g}_{KCa}m_{KCa}Ca_{iL}\ (V - E_{KCa})$ if $0.004\ \bar{g}_{KCa} < 0.0000001$. Otherwise, $I_{KCa} = \bar{g}_{KCa}m_{KCa}\ (V - E_{KCa})$. *Permeability values for the calcium currents I_T and I_L are in 10^{-9} cm^3/s. $I_{KirNoNS}$, I_{Kir} without negative slope in the steady-state *I/V* relationship.

$$dm_i/dt = \left[m_{i\infty}(V) - m_i\right]/\tau_{mi}(V) \quad (7)$$

$$dh_i/dt = \left[h_{i\infty}(V) - h_i\right]/\tau_{hi}(V) \quad (8)$$

where $m_{i\infty}(V)$, $h_{i\infty}(V)$, $\tau_{mi}(V)$, and $\tau_{hi}(V)$ are the steady-state and time constants of activation and inactivation for a given current I_i. The expressions for these steady-state and time constants are given in Table 1, together with the default parameter values (those used in the last section of RESULTS). Parameter values subjected to analysis are specified in the main text of RESULTS and corresponding figure legends.

The calcium-dependent potassium current I_{AHP} and the voltage- and calcium-dependent potassium current I_{KCa} were gated by the variation of intracellular calcium linked to activation of the high-threshold calcium current I_L, whereas the calcium-dependent cationic current I_{CAN} was gated by the variation of intracellular calcium linked to activation of I_T. Intracellular calcium dynamics, in turn, was modeled as previously (Amarillo et al. 2014; McCormick and Huguenard 1992) with a simple diffusion model from a shell of 100-nm depth just beneath the plasma membrane with the dimensions of the model cell (22,700 μm^2). The equation that describes this diffusion is

$$dCa_i/dt = -\left(I_T \text{ or } I_L\right)/\text{depth}/F/2\left(0.0000001\right) + \left(Ca_i0 - Ca_i\right)/\beta \quad (9)$$

where depth is the thickness of the shell, F is the Faraday constant, Ca_i0 is the initial calcium concentration (50 nM), and β is the diffusion rate (1 ms).

Addition of the calcium-dependent cationic current I_{CAN} was necessary to reproduce the decaying plateau potentials that follow LTSs observed experimentally. I_{CAN} was adapted from Zhu et al. (1999) with the parameters listed in Table 1.

Slice preparation and electrophysiology. All experiments were carried out in accordance with the National Institutes of Health *Guide for the Care and Use of Laboratory Animals* and were approved by the Institutional Committee for the Care and Use of Laboratory Animals (CICUAL) of the National Atomic Energy Commission of Argentina (CNEA). All procedures for obtaining brain slices and for electrophysiological recording have been previously described (Amarillo et al. 2008, 2014).

Briefly, brain slices were prepared from 2- to 4-wk-old NIH Swiss mice. After induction of deep anesthesia with pentobarbital sodium (50–75 mg/kg ip), mice were decapitated and the brains were removed into an ice-cold oxygenated artificial cerebrospinal fluid (ACSF) that contained (in mM) 126 NaCl, 2.5 KCl, 1.25 Na_2PO_4, 26 $NaHCO_3$, 2 $CaCl_2$, 2 $MgCl_2$, and 10 dextrose. The brain was blocked at a coronal plane, and 350-μm-thick slices were cut with a manual vibroslicer (WPI, Sarasota, FL). Slices including the ventrobasal thalamic nuclei were incubated at 30°C for 1 h and thereafter maintained at room temperature in oxygenated ACSF (95% CO_2, 5% O_2) until they were transferred to the recording chamber continuously perfused with oxygenated ACSF.

Neurons from ventrobasal thalamic nuclei (ventral posterolateral and ventral posteromedial nucleus) were visualized with a CCD camera (Panasonic, Newark, NJ) mounted on a Carl Zeiss Axioskop FSII plus fixed-stage microscope (Carl Zeiss, Oberkochen, Germany) equipped with IR-DIC optics. Patch pipettes were made from borosilicate glass in a Sutter P-1000 horizontal puller (Sutter Instrument, Novato, CA) with resistances between 2 and 5 MΩ and filled with an intracellular solution containing (in mM) 119 CH_3KO_3S, 12 KCl, 1 $MgCl_2$, 0.1 $CaCl_2$, 1 EGTA, 10 HEPES, 0.4 Na-GTP, and 2 Mg-ATP, pH 7.4. Neurons were recorded in fast current-clamp mode with an Axoclamp 700B amplifier (Molecular Devices, Sunnyvale, CA) after stabilization of the resting membrane potential. Recordings were low-pass filtered at 10 KHz, pipette capacitance was canceled, and bridge balance was compensated. A sampling rate of 10 kHz was used; data were acquired on a personal computer with pCLAMP10 software (Molecular Devices) and stored for further analysis.

Dynamic clamp. Dynamic clamp was implemented with a dedicated DAQ card PCIe-6351 (National Instruments, Austin, TX) that was commanded by the open source software StdpC under the Windows 7 OS (Kemenes et al. 2011). The analog output of the MultiClamp 700B amplifier was connected to analog inputs on both the acquisition card Digidata 1440a (Molecular Devices) and the dynamic clamp card PCIe-6351. This signal was used to track the membrane potential with the acquisition software pCLAMP10 as well as the voltage input for implementing the dynamic-clamp loop. Analog outputs of the two interface cards were connected to a custom-made real-time voltage summing device (Patent P20170101319, CONICET, Argentina), whose output was connected, in turn, to the analog input of the amplifier. This configuration allows us to simultaneously perform current-clamp protocols with the pCLAMP10 software and dynamic-clamp simulations with the StdpC software in the MultiClamp 700B amplifier.

RESULTS

The unique biophysical properties of I_{Kir} induce bistability of the membrane potential. The inward rectification profiles of potassium channels of the Kir2.X family show a distinctive region of negative slope in the *I/V* relationship (Dhamoon et al. 2004). This property of Kir channels is produced by the voltage-dependent block of the channel pore by intracellular Mg^{2+} and polyamines (reviewed in Anumonwo and Lopatin 2010). We have previously identified Kir2.2 as the main ion channel subunit responsible for I_{Kir} in TC neurons (Amarillo et al. 2014). Currents produced by Kir2.2 channels in heterologous systems show the strongest voltage-dependent inward rectification compared with those produced by Kir2.1 and Kir2.3 channels (Dhamoon et al. 2004). Accordingly, TC neurons display a fast inward rectification that is not present on TC cells from Kir2.2-knockout mice or when Kir channels are blocked by low concentrations of barium (10–50 μM) (Amarillo et al. 2014).

In TC neurons from mice, the shape of the total subthreshold steady-state *I/V* curve is determined by the combined contribution of seven conductances (Amarillo et al. 2014). We started by analyzing a model that includes I_{Kir} (modeled based on data from TC neurons from mice; Amarillo et al. 2014) and the potassium and sodium leak conductances. The steady-state *I/V* relationship for the leaks alone (Fig. 1*A*) is linear, whereas the steady state *I/V* relationship for I_{Kir} shows strong inward rectification and a negative slope conductance region between −85 mV and −60 mV (Fig. 1*A*). For a certain combination of conductance values of Kir and leaks (see figure legend), the *I/V* curve of this I_{Kir}-Leaks minimal model is nonmonotonic (Fig. 1*A*) and the steady-state *I/V* curve crosses the zero current axis at three values of membrane potential (Fig. 1*A*). For a one-dimensional system, this *I/V* curve gives rise to a saddle node bifurcation (Izhikevich 2005) with two stable equilibrium points (Fig. 1*A*, *a* and *c*) separated by one unstable equilibrium point (Fig. 1*A*, *b*). The consequence of this dynamical property is the expression of membrane potential bistability. Figure 1*B* shows the simulated evolution in time of the membrane potential for the I_{Kir}-Leaks minimal model for six different initial membrane potential values, around the unstable equilibrium point. For the three initial values that are above the unstable point (−74.6 mV) the membrane potential evolves toward the depolarized stable equilibrium (−57.7 mV), whereas for the other three values the mem-

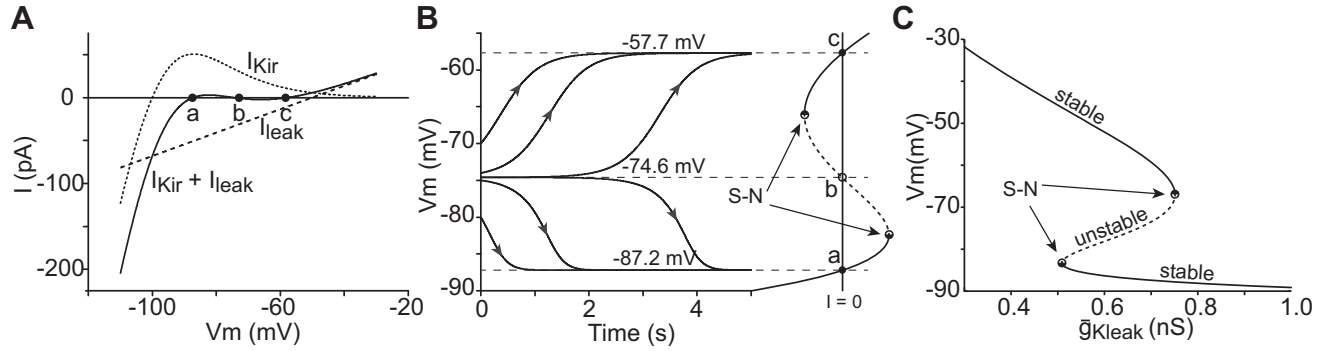

Fig. 1. The Kir current induces bistability of the membrane potential (V_m). *A*: simulated steady-state current-voltage (*I/V*) relationships of the I_{Kir}-Leaks model cell with parameters adjusted to generate bistability in the absence of current injection. $\bar{g}_{Kir}$ = 15.9 nS, $\bar{g}_{Kleak}$ = $\bar{g}_{Naleak}$ = 0.68 nS, E_{Na} = 0 mV, and E_K = −100 mV. The combined I_{Kir}-Leaks *I/V* curve (solid trace) crosses the zero current level at 3 different voltage values (*points a–c*). *B*: simulated time course of V_m for the model in *A* for 6 different initial V_m values (from negative to positive: −80, −75, −74.7, −74.5, −74, and −70 mV). Projected on *right* is the bifurcation diagram using current injection (I_{inj}) as the bifurcation parameter. The *V/I* curve crosses zero current at the stable *points a* and *c* and at the unstable *point b* (same V_m values as in *A*). Dashed segment indicates instability, and solid segments indicate stability. S-N indicates the saddle node bifurcation points. *C*: bifurcation diagram of the I_{Kir}-Leaks model in *A* using $\bar{g}_{Kleak}$ as the bifurcation parameter.

brane potential stabilizes at the hyperpolarized stable equilibrium (−87.2 mV). This bistability is further evidenced when shown vis à vis the bifurcation diagram of the I_{Kir}-Leaks model at injected current = 0 (Fig. 1*B*, *right*).

The physiological modulation of the potassium leak current by neurotransmitters is considered the mechanism that controls the resting membrane potential of TC neurons (McCormick and Prince 1987, 1988). For this reason, we analyzed the effect of varying the potassium leak maximum conductance ($\bar{g}_{Kleak}$) on the dynamical behavior of the I_{Kir}-Leaks model. Similarly to using current injection as the bifurcation parameter, changing $\bar{g}_{Kleak}$ displays two saddle node bifurcation points and a region of instability in the bifurcation diagram (Fig. 1*C*).

Interaction of amplifying I_{Kir} and resonant I_h generates sustained subthreshold oscillations. The hyperpolarization-activated cationic current I_h plays an important role in establishing the resting membrane potential and modulating the oscillations mediated by the low-threshold calcium current I_T in TC neurons (Amarillo et al. 2015; McCormick and Pape 1990b; Soltesz et al. 1991). I_h adds robustness to the repetitive LTSs by potentiating the initial phase of depolarization. In addition, the resonant activation of I_h allows transient, negative excursions of the membrane potential between LTSs; without this recovering mechanism, the membrane potential would stabilize at the more negative total steady-state conductance level (Amarillo et al. 2015).

The interaction of a resonant current such as I_h with an amplifying current such as I_{Kir} can theoretically support periodic subthreshold oscillations (Izhikevich 2005). In striatal cholinergic interneurons, these two hyperpolarization-activated currents underlie the cyclic transient hyperpolarizations that generate the interburst intervals in these neurons (Wilson 2005). In agreement with these results, we have previously shown that the I_{Kir}-I_h-Leaks minimal model exhibits sustained oscillations (Amarillo et al. 2014). Figure 2*A* shows the time course of the changes in the membrane potential produced by this two-dimensional model (dV/dt and dm_h/dt) for a maximum conductance of Kir of 41 nS and physiological values of maximum conductances of *h* and the leaks ($\bar{g}_h$ = 5 nS; $\bar{g}_{Kleak}$ = 2.3 nS; $\bar{g}_{Naleak}$ = 0.7 nS). At rest—with zero current injection—the membrane potential stabilizes at −82.66 mV. The injection of a current of 60 pA induces robust periodic oscillations that are not observed with injection of either 40 pA (damped oscillations) or 80 pA. The phase-plane portrait of these three conditions (Fig. 2*B*) shows that *1*) the trajectory of the dampened oscillations (*top* gray trajectory and V-nullcline) obtained with injection of 40 pA coalesces to a stable focus; *2*) the orbit of the oscillations obtained with 60 pA (*middle* black trajectory and V-nullcline) enters a stable limit cycle around an unstable focus; and *3*) the membrane potential stabilizes at a depolarized stable focus when the current injection is 80 pA (*bottom* gray trajectory and V-nullcline). In the three cases, the voltage and I_h activation nullclines (m_h, steady-state activation curve for the h current) intersect in a single focus, which is either stable or unstable. This indicates that the transition from either of the two stable foci to the unstable focus occurs via a Hopf bifurcation, as shown in Fig. 2*C*. The bifurcation diagram in Fig. 2*C* shows the two Hopf bifurcation points and the amplitude of the limit cycle as the current injection changes. At the bifurcation points, the gradually increasing/decreasing amplitude of the limit cycle indicates that both transitions occur via supercritical Hopf bifurcations.

As mentioned in *The unique biophysical properties of I_{Kir} induce bistability of the membrane potential*, physiological changes in $\bar{g}_{Kleak}$ induce changes in the resting membrane potential of TC neurons. To examine the range of values of $\bar{g}_{Kleak}$ that induce oscillations, we performed the bifurcation analysis using $\bar{g}_{Kleak}$ as the bifurcation parameter (Fig. 2*D*). The system enters a stable limit cycle via a supercritical Hopf bifurcation as $\bar{g}_{Kleak}$ is decreased. Between this bifurcation point ($\bar{g}_{Kleak}$ ≈1.1 nS) and a $\bar{g}_{Kleak}$ value of ≈0.4 nS, the membrane potential is unstable. At this last point, the limit cycle disappears via a saddle node on invariant circle bifurcation (S-NIC). This last bifurcation allows the system to undergo oscillations at low frequencies (Izhikevich 2005), providing a possible mechanism to generate physiological or pathological slow rhythms (<1 Hz) (Fig. 2*D*, *inset*).

Effect of I_{Kir} on dynamics of a reduced model of thalamocortical neurons. The low-threshold calcium current I_T is absolutely required for burst firing in TC neurons, as evidenced by both pharmacological (Dreyfus et al. 2010) and genetic ablation (Kim et al. 2001) studies. The interaction between the amplifying activation variable m_T and the resonant inactivation variable h_T of I_T creates an oscillatory unit that can support

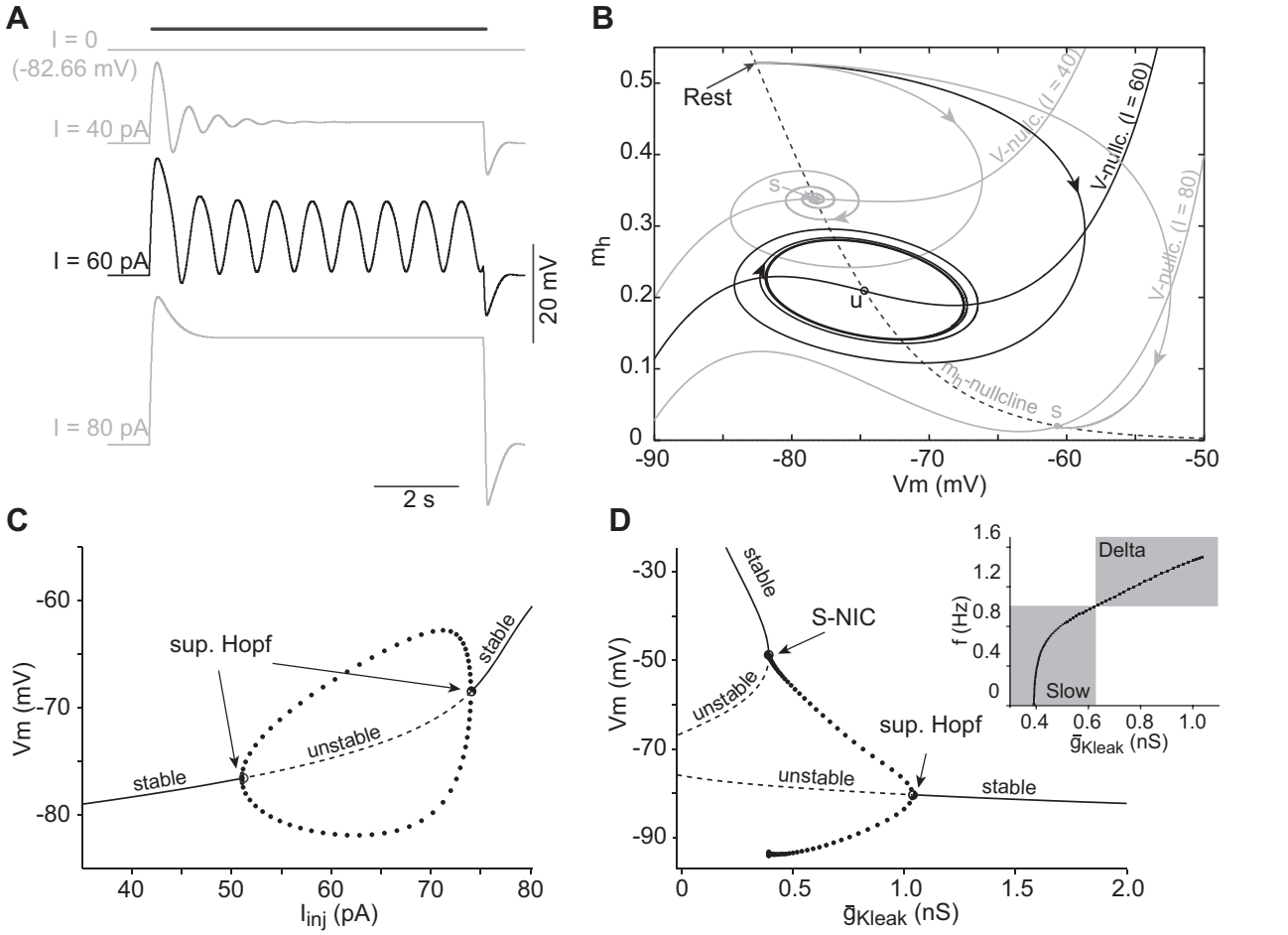

Fig. 2. Interaction of I_{Kir} and I_h induces robust sustained subthreshold oscillations. *A*: time course of the membrane potential produced by the I_{Kir}-I_h-Leaks model cell for different current injection magnitudes (indicated on *left* of each trace). Simulations were initiated at the resting membrane potential (−82.66 mV; $I = 0$), and the injected current was applied during the time indicated by the bar above *top* trace. $\bar{g}_{Kir} = 41$ nS, $\bar{g}_h = 5$ nS, $\bar{g}_{Kleak} = 2.27$ nS, and $\bar{g}_{Naleak} = 0.68$ nS. Gray traces indicate evolution toward a stable equilibrium and black trace indicates sustained oscillations. *B*: phase-plane portrait for the 3 current levels shown in *A*, starting at rest [current injection (I_{inj}) = 0]: 40 pA, 60 pA, and 80 pA (gray and black have same meaning as in *A*). Note that for the 3 conditions the nullclines intersect in a single point: stable foci (s) for 40 and 80 pA and an unstable focus (u) for 60 pA. *C*: bifurcation diagram as I_{inj} changes showing the 2 supercritical Hopf bifurcation points (sup. Hopf) and the amplitude of the limit cycle (dots). *D*: bifurcation analysis using $\bar{g}_{Kleak}$ as the bifurcation parameter. At the saddle node on invariant circle bifurcation (S-NIC) point, the stable limit cycle appears/disappears as $\bar{g}_{Kleak}$ increases/decreases because of the presence of a saddle node bifurcation that shrinks/expands a small heteroclinic trajectory (Izhikevich 2005). *Inset*: frequency (f) of the limit cycle as function of $\bar{g}_{Kleak}$: f decreases as $\sqrt{\bar{g}_{Kleak} - \bar{g}_{Kleak}b}$ when $\bar{g}_{Kleak}$ decreases (from *right* to *left*) toward the bifurcation value $\bar{g}_{Kleak}b$. Separation between slow and delta bands (at 1 Hz) is indicated by the shadowed area.

sustained oscillations (repetitive LTSs; Amarillo et al. 2014; Hutcheon and Yarom 2000). The other subthreshold conductances expressed by TC neurons modulate the generation, repetitiveness, repolarization, frequency, and voltage range of the LTSs produced by I_T (Amarillo et al. 2014, 2015).

In TC neurons, the oscillatory system formed by I_{Kir}-I_h described in *Interaction of amplifying I_{Kir} and resonant I_h generates sustained subthreshold oscillations* coexists with the oscillatory system formed by the gating variables of I_T. We sought to examine how the interaction between the different modeled components of these two oscillatory systems impacts on the dynamics of the membrane potential. We have previously shown that the depolarizing drive contributed by I_h in the I_T-I_h-Leaks model not only adds to the regenerative activation of I_T during the ascending phase of the LTS, giving rise to larger and faster oscillations, but also permits the occurrence of LTSs at more hyperpolarized potentials (Amarillo et al. 2015). Including I_{Kir} (9 nS; Fig. 3*A*) in that model does not change the dynamical properties of the system, which transits between stability and instability via a subcritical Hopf bifurcation at hyperpolarized potentials and via a supercritical Hopf bifurcation at depolarized levels, either in the presence or absence of I_{Kir} (Fig. 3*A*). Yet there are quantitative changes after addition of I_{Kir} to the I_T-I_h-Leaks model: First, there is a positive shift in the range of current injections such that, in the presence of I_{Kir}, no current injection is required to produce maximum-amplitude oscillations (see oscillations produced at zero current value, i.e., resting state, in Fig. 3*A*). These results indicate that I_{Kir} endows the system with the ability to oscillate spontaneously at lower levels of I_T (see DISCUSSION). Second, the minimum value of permeability of I_T (p_T) required to generate sustained LTSs decreases from 12.8×10^{-9} cm^3/s to 10.7×10^{-9} cm^3/s. When we performed the bifurcation analysis using the maximum permeability of I_T as the bifurcation parameter (for $I = 0$), in both the presence and absence of I_{Kir}, we were able to visualize the effect of I_{Kir} on the range of permissive p_T

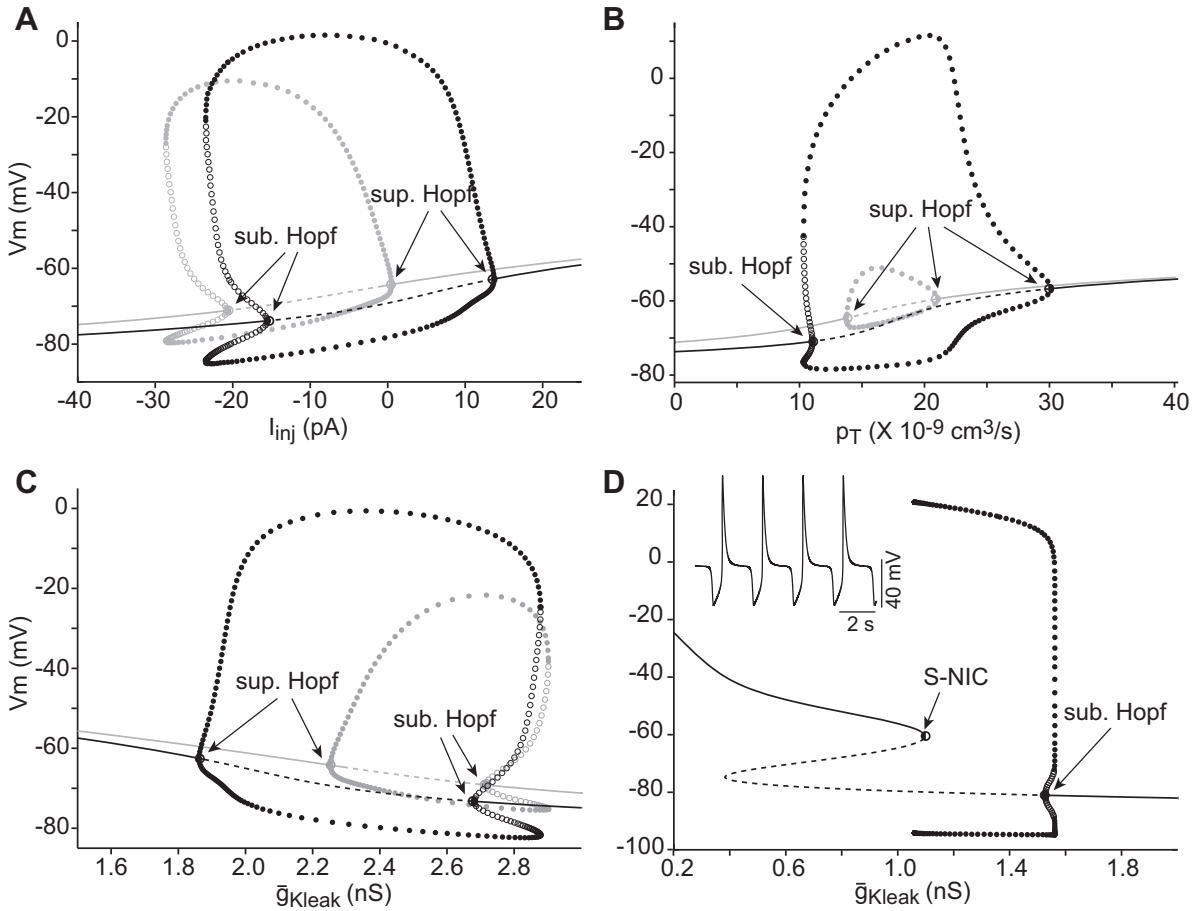

Fig. 3. Effect of I_{Kir} on the dynamics of a model of thalamocortical neurons that includes I_h and I_T. *A*: bifurcation diagram of the I_T-I_h-Leaks model using current injection (I_{inj}) as the bifurcation parameter, in the presence of I_{Kir} (9 nS, black diagram) or in the absence of I_{Kir} (gray diagram). Identical parameter values were used for the other conductances: $\bar{g}_h$ = 5 nS, $\bar{g}_{Kleak}$ = 2.27 nS, $\bar{g}_{Naleak}$ = 0.68 nS, and maximum permeability (p_T) = 14×10^{-9} cm^3/s. sub. Hopf and sup. Hopf indicate subcritical and supercritical Hopf bifurcation points, respectively. Dots are max/min of stable (filled dots) or unstable (open dots) limit cycle. V_m, membrane potential. *B*: bifurcation diagram of the I_T-I_h-Leaks model using the maximum permeability of I_T (p_T) as the bifurcation parameter in the presence of I_{Kir} (9 nS, black diagram) or in the absence of I_{Kir} (gray diagram). *C*: bifurcation diagram of the I_T-I_h-Leaks model using $\bar{g}_{Kleak}$ as the bifurcation parameter in the presence of I_{Kir} (9 nS, black diagram) or in the absence of I_{Kir} (gray diagram). *D*: bifurcation diagram of the I_T-I_h-Leaks model using $\bar{g}_{Kleak}$ as the bifurcation parameter in the presence of I_{Kir} (41 nS). *Inset*: time course of V_m oscillations at a $\bar{g}_{Kleak}$ value that is very close to the bifurcation point ($\bar{g}_{Kleak}$ = 1.05973610281 nS). Conventions and parameter values for the other conductances in *B–D* are as in *A*.

values (i.e., values of p_T that allow sustained oscillations) (Fig. 3*B*). Without current injection, p_T is permissive for values between 12×10^{-9} cm^3/s and 30×10^{-9} cm^3/s when using a $\bar{g}_{Kir}$ of 9 nS (Fig. 3*B*), whereas in the absence of I_{Kir} these permissive p_T values are between 14×10^{-9} cm^3/s and 22×10^{-9} cm^3/s (Fig. 3*B*). The amplitude of the membrane potential oscillations is notably larger in the presence of I_{Kir}.

When using $\bar{g}_{Kleak}$ as the bifurcation parameter without current injection, the system has two different dynamical behaviors depending on the magnitude of $\bar{g}_{Kir}$: At low levels of $\bar{g}_{Kir}$ (9 nS), the transitions between rest and the limit cycle occur via Hopf bifurcations (Fig. 3*C*), similar to the behavior of the system in the absence of I_{Kir} (Fig. 3*C*). Addition of low magnitudes of I_{Kir} again produces a quantitative effect by increasing the range of permissive values of $\bar{g}_{Kleak}$. On the other hand, for high values of $\bar{g}_{Kir}$ (41 nS; Fig. 3*D*), the limit cycle disappears via a S-NIC bifurcation as $\bar{g}_{Kleak}$ decreases. As mentioned above, this S-NIC bifurcation endows the system with the ability to oscillate at very slow frequencies. Curiously, for values of $\bar{g}_{Kleak}$ infinitesimally close to the bifurcation point, the time course changes from the typical triangle-shaped oscillations to oscillations with prolonged plateaus after the LTSs (Fig. 3*D*, *inset*), as seen in recordings from rodent TC neurons in vitro (see below).

Negative slope conductance region of I/V curve is key pro-oscillatory feature of I_{Kir}. To confirm that the negative slope conductance region of the *I/V* curve of I_{Kir} is responsible for promoting the oscillatory behavior of the membrane potential of TC neurons, we examined the effect of eliminating this region of negative slope of the *I/V* curve of I_{Kir} (Fig. 4*A*) in the three models of increasing complexity described above. As expected, bistability does not occur in the minimal I_{Kir}-leaks model with a modified Kir current that lacks the negative slope conductance region because in this case the *I/V* curve is always monotonic (i.e., all the points are stable) (Fig. 4*A*). The bifurcation analysis using this modified Kir in the I_{Kir}-I_h-Leaks and I_{Kir}-I_h-I_T-Leaks models (Fig. 4, *B* and *C*, respectively) shows that no oscillations (limit cycles) are present when Kir lacks the negative slope conductance. A Kir conductance without negative slope is persistently active at depolarized membrane potentials, and hence the slope of the V/I_{inj} curve decreases and flattens (Fig. 4, *B* and *C*). To exclude the possibility that the

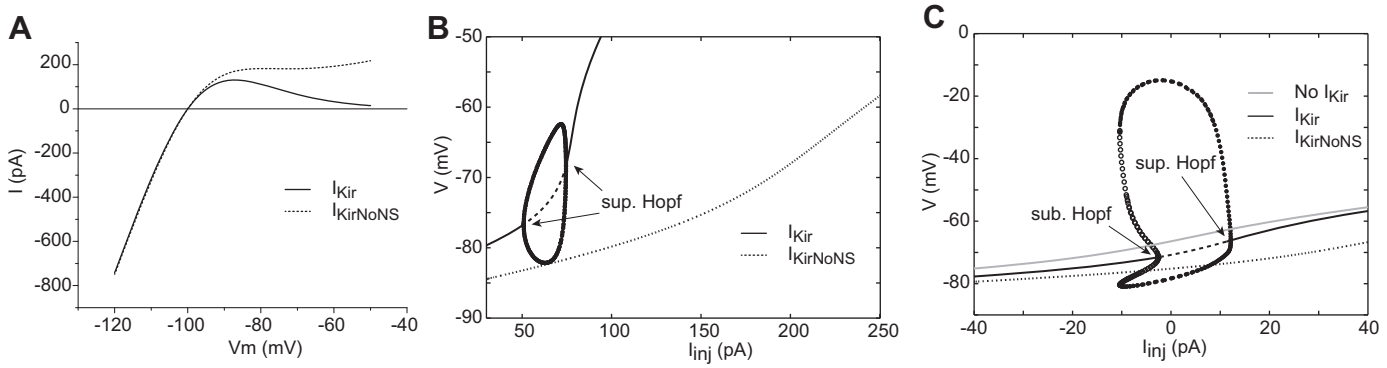

Fig. 4. Effect of the negative slope conductance region of the *I/V* curve of I_{Kir} on the dynamics of TC neuron models. *A*: simulated *I/V* curves of I_{Kir} with (I_{Kir}, solid line) and without ($I_{KirNoNS}$, dotted line) negative slope conductance (see METHODS). *B*: bifurcation diagram, using current injection (I_{inj}) as the bifurcation parameter, of the I_{Kir}-I_h-Leaks model with (black solid/dashed line and max/min of limit cycle) and without (dotted line) negative slope conductance ($\bar{g}_{Kir}$ = 41 nS, $\bar{g}_h$ = 5 nS, $\bar{g}_{Kleak}$ = 2.27 nS, and $\bar{g}_{Naleak}$ = 0.68 nS). *C*: comparison of the bifurcation diagrams of the 3 models: *1*) I_h-I_T-Leaks (No I_{Kir}, gray), *2*) I_{Kir}-I_h-I_T-Leaks with Kir with negative slope (black solid/dashed line and max/min of limit cycle), and *3*) $I_{KirNoNS}$-I_h-I_T-Leaks with Kir without negative slope (dotted line), using I_{inj} as the bifurcation parameter and physiological values for all conductances ($\bar{g}_{Kir}$ = 9 nS, $\bar{g}_h$ = 5 nS, $\bar{g}_{Kleak}$ = 2.27 nS, $\bar{g}_{Naleak}$ = 0.68 nS, and $p_T = 11.3 \times 10^{-9}$ cm^3/s).

lack of periodicity is due to an increased requirement of depolarizing current we expanded the range of injected current, and yet no limit cycle was observed (Fig. 4*B*).

Increasing maximum conductance of I_{Kir} induces sustained repetitive burst firing in TC neurons from mice. Recorded membrane potential of TC neurons from mice is stable at about −67 mV. In recordings performed in brain slices from rodents, it is very rare to observe spontaneous repetitive bursting without manipulating the extracellular concentration of divalent ions and/or without stimulating the cortico-thalamic/reticulo-thalamic afferents (Jacobsen et al. 2001; Leresche et al. 1991; Warren et al. 1994). Moreover, in typical experiments in rodent brain slices, even sustained injection of current in the depolarizing or hyperpolarizing direction does not induce oscillations at subthreshold levels. Larger magnitudes of depolarizing current (suprathreshold depolarization) elicit either tonic firing or single-burst firing depending on the membrane potential before the onset of the stimulus (holding potential). Either mode of firing is dependent on the level of inactivation of the low-threshold calcium current I_T, which reflects the history of the membrane potential. At depolarized holding potentials, T channels are inactivated and the neuron responds with a train of action potentials at a frequency that correlates with the magnitude of the injected current. At holding potentials negative to about −65 mV, T channels are increasingly deinactivated and the neuron responds to a depolarizing input with a low-threshold calcium spike (LTS), crowned by a burst of Na^+/K^+-mediated action potentials (see recordings of TC neurons from rodents elsewhere; for example, Amarillo et al. 2014; Kim et al. 2001; Llinás and Jahnsen 1982; Meuth et al. 2006; Zhu and Uhlrich 1998). To test the predicted prooscillatory effect of I_{Kir}, we recorded 19 TC neurons in the ventrobasal nuclei of the thalamus from mice and manipulated the maximum conductance of Kir with dynamic clamp ($d\bar{g}_{Kir}$, see METHODS). In all tested cells, sole introduction of artificial I_{Kir} induces repetitive burst firing (examples from 3 different cells are shown in Fig. 5*A*, Fig. 5*B*, and Fig. 7*A*). The range of minimal values of $d\bar{g}_{Kir}$ that induced oscillations was 8–53 nS, with a mean (± SD) of 23.9 ± 9.8 nS (19 cells). The shape of the burst cycle changes depending on the magnitude of artificial $\bar{g}_{Kir}$ introduced by dynamic clamp (Fig. 5*A*). For the minimal $d\bar{g}_{Kir}$ that induces oscillations, the cycle consists of an initial hyperpolarization followed by a slow recovering depolarization that brings the membrane potential to the LTS threshold. Immediately after the LTS, the next cycle reinitiates with a similar sequence. In contrast, for larger $d\bar{g}_{Kir}$ magnitudes, a plateau potential of varying lengths follows the LTSs, introducing a delay to the hyperpolarization that initiates the next cycle (Fig. 5*A*, 24 and 30 nS). A similar response was obtained by varying the magnitude of injected hyperpolarizing current for a large value of $d\bar{g}_{Kir}$ (50 nS; Fig. 5*B*). The plateau potential is only observed for current injections around threshold level (–30 pA), and not for larger hyperpolarizations (–60 pA). A large hyperpolarization (–90 pA) overpowers the amount of artificial $d\bar{g}_{Kir}$ introduced by dynamic clamp, and no subthreshold oscillations are observed (Fig. 5*B*, *bottom right*).

We have previously estimated that the maximum conductance of native Kir in most TC neurons is ~5 nS (Amarillo et al. 2014, yet there is significant variability among some cells). This was done by subtracting the *I/V* curves in the presence and absence of barium, which is considered a specific blocker of Kir 2.X channels at low concentrations (Dhamoon et al. 2004; Schram et al. 2003). Here we used dynamic clamp to reinstate the endogenous levels of $\bar{g}_{Kir}$—and hence the fast inward rectification—in TC cells that had been treated with 10 μM barium. Figure 5*C* shows that the characteristic fast rectification of TC neurons (control; Fig. 5*C*, *top left*) is lost in the presence of 10 μM barium (Fig. 5*C*, *top right*), and it is subsequently reconstituted after reintroduction of I_{Kir} with dynamic clamp (Fig. 5*C*, *bottom*). In agreement with our previous estimations, the $d\bar{g}_{Kir}$ magnitude that restores the fast inward rectification was 5 nS in two cells tested (one is shown in Fig. 5*C*, *bottom left*) and 7 nS in another cell. A larger amount (15 nS in this cell) endows TC neurons with a stronger inward rectification (i.e., amplification of hyperpolarization; Fig. 5*C*, *bottom right*) and slow oscillations (repetitive bursts are truncated by finalization of current injection steps in Fig. 5*C*, *bottom right*). Figure 5*D* shows the *I/V* curves for the same TC neuron recorded in Fig. 5*C* under the different conditions described above: control, 10 μM barium, and 10 μM barium + 5 nS or 15 nS $d\bar{g}_{Kir}$.

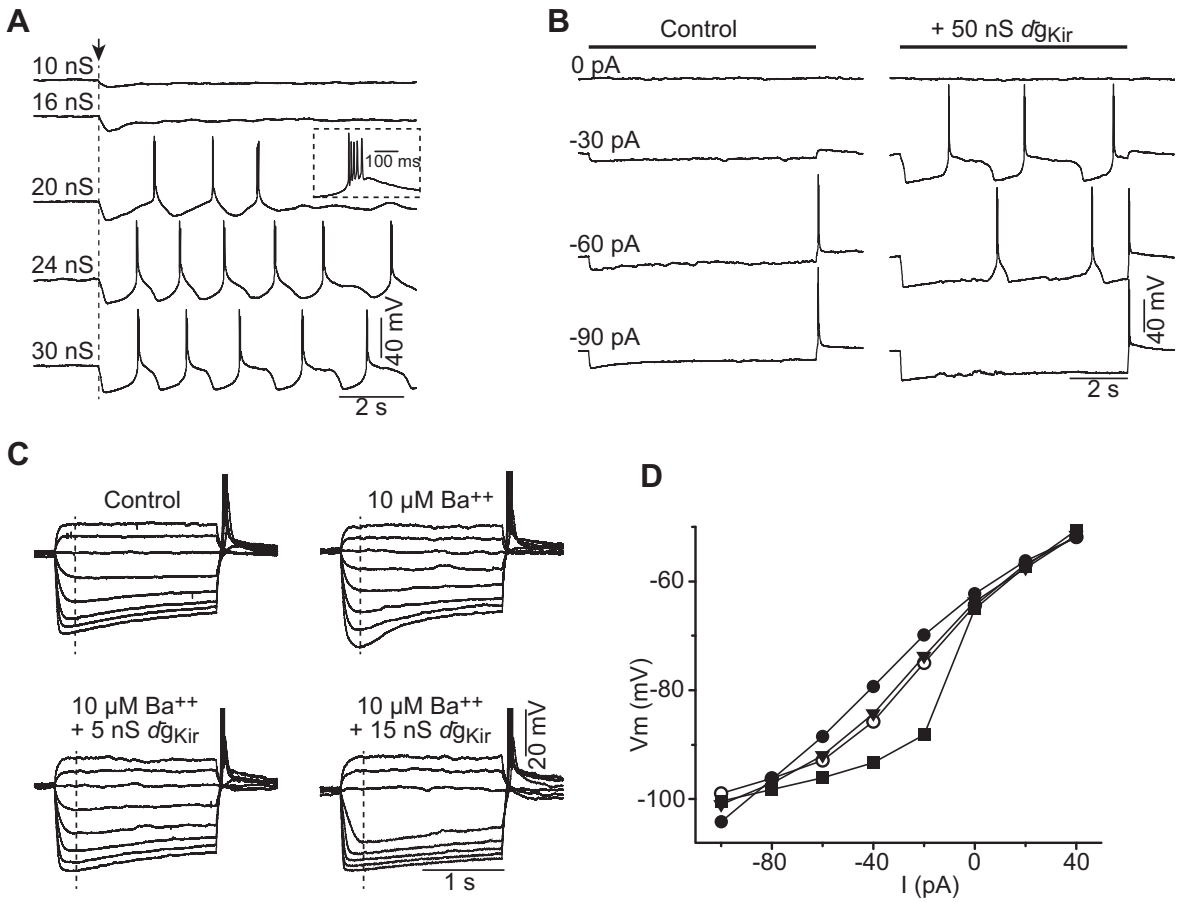

Fig. 5. Artificial increase of $\bar{g}_{Kir}$ induces sustained repetitive burst firing in TC neurons from mice. *A*: current-clamp recordings of a TC neuron from the ventrobasal complex of mouse thalamus, where different amounts of maximum conductance of Kir, ranging from 10 to 30 nS, were artificially introduced with dynamic clamp (arrow and vertical dashed line indicate onset of dynamic clamp). *Inset*: a magnified view of 1 of the bursts of action potentials riding on a low-threshold spike. *B*: current-clamp recordings of a different TC neuron in response to increasing magnitudes of injected hyperpolarizing current before (*left*) and after (*right*) introduction of 50 nS of $\bar{g}_{Kir}$ with dynamic clamp. *C*: current-clamp recordings of another TC neuron with a protocol of square pulses in 20-pA increments from –100 pA, under control conditions (*top left*) and after bath application of 10 μM barium (*top right*). Note the disappearance of the fast inward rectification (measured at an early time point, vertical dashed line) after application of Ba^{2+}. *Bottom left* traces show the rescue of the fast inward rectification after introduction of 5 nS of $\bar{g}_{Kir}$ with dynamic clamp. An excess of d$\bar{g}_{Kir}$ (15 nS) further increases the fast inward rectification in this cell (*bottom right*). *D*: current/voltage curves for the same TC neuron recorded in *C* under these different conditions, measured at the time indicated by vertical dashed lines in *C*. ○, Control; ●, 10 μM barium; ▼, 10 μM barium + 5 nS d$\bar{g}_{Kir}$; ■, 10 μM barium + 15 nS d$\bar{g}_{Kir}$.

Endogenous I_{Kir} promotes repetitive bursting in mouse TC neurons. As mentioned above, TC neurons in the mouse do not display slow intrinsically generated oscillations in vitro (in contrast to what is observed in carnivorous species such as cat and ferret). It has been shown previously that adding artificial I_T induces slow oscillations in all TC neurons recorded in vitro (Hughes et al. 2009), a finding that is consistent with theoretical predictions (Amarillo et al. 2014, 2015; Rush and Rinzel 1994). We implemented this method to induce oscillations in TC neurons from mice in coronal slices (Fig. 6). We introduced with dynamic clamp the minimal I_T maximum conductance that induces slow oscillations in the three TC neurons (40, 55, and 70 nS; the latter is shown in Fig. 6) and tested whether these oscillations were sensitive to pharmacological blockade of I_{Kir}. As expected, adding 10 μM Ba^{2+} eliminated the oscillations in all three cells. Furthermore, oscillations were rescued by adding physiological magnitudes of d$\bar{g}_{Kir}$ (5, 7, and 8 nS, respectively; Fig. 6). This result indicates that the intrinsic magnitude of $\bar{g}_{Kir}$ expressed by TC neurons from mice is able to promote slow oscillations when the appropriate balance among all the subthreshold conductances is provided. This is also consistent with the bifurcation analysis of the model that includes the two oscillatory systems, m_T-h_T and I_{Kir}-I_h (Fig. 3), in which the presence of low levels of I_{Kir} increases the range of permissive values of p_T.

Role of I_{Kir} in oscillatory behavior of TC neurons. To further explore the mechanism by which increasing I_{Kir} in rodent TC neurons induces repetitive burst firing, we examined the membrane potential time course of induced repetitive bursts (Fig. 7*A*, *top*) at the same time that we recorded the Kir current injected by the dynamic clamp system (Fig. 7*A*, *bottom*). As expected from previous computational analysis (Amarillo et al. 2014), I_{Kir} decreases as the membrane potential recovers toward the base of the LTS, reaching its minimal value during the LTSs and the bursts of action potentials. After the firing of the LTS, the magnitude of I_{Kir} began to increase during the slow initial hyperpolarization that follows the LTS (plateau potential) until an inflection point (Fig. 7*A*), at which the activation of I_{Kir} becomes regenerative and thus increases abruptly to its maximum value. This is mirrored in the membrane potential by a sudden hyperpolarization, which removes the inactivation of I_T at the same time that it induces the

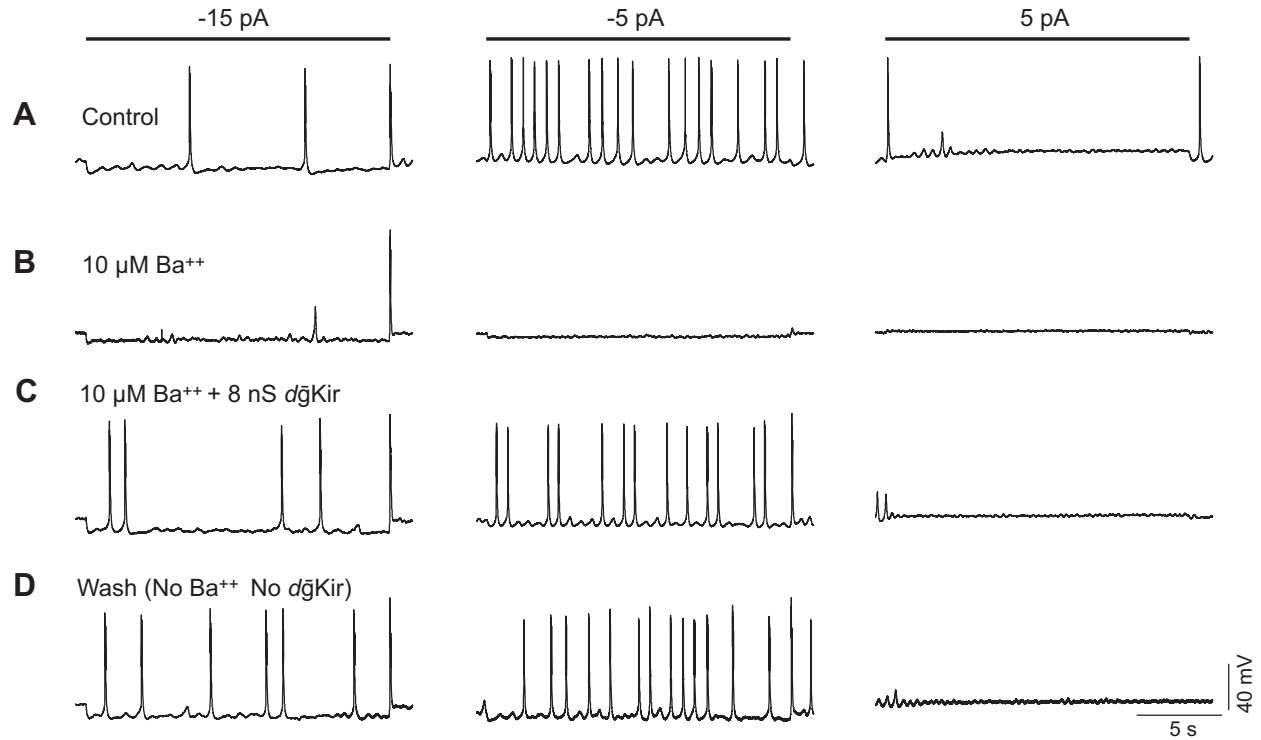

Fig. 6. Intrinsic $\bar{g}_{Kir}$ levels promote repetitive bursting in TC neurons. *A*: repetitive bursting induced by adding artificial I_T with dynamic clamp to a TC neuron. Oscillations are more readily elicited at rest (−70 mV, not shown) and at slightly hyperpolarized membrane potentials [current injection (I_{inj}) = −5 pA]. *B*: blockade of I_{Kir} with a low concentration of Ba^{2+} (10 μM) eliminates oscillations induced by artificial I_T. *C*: reinstating I_{Kir} ($d\bar{g}_{Kir}$ = 8 nS) with dynamic clamp in the presence of Ba^{2+} (10 μM) rescues repetitive bursting induced by artificial I_T. *D*: the neuron recovers the original (control) induced oscillatory behavior after washout of Ba^{2+} in the absence of $d\bar{g}_{Kir}$. A maximum conductance value = 70 nS for I_T was used in all conditions (see METHODS).

activation of I_h. To closely examine the interaction among I_{Kir}, I_h, and the gating variables of I_T during this process, we used a more complete model of TC neurons—which includes all the subthreshold conductances as well as the suprathreshold conductances that generate and control Na^+/K^+ spiking—to reproduce the time course of induced oscillations (Fig. 7, *B* and *C*; also see METHODS and Table 1). To test the possibility that I_{Kir} could mediate the very slow oscillations and the plateau potentials observed experimentally by a mechanism involving a S-NIC bifurcation as in Fig. 2*D* and Fig. 3*D*, we first tried to reproduce the time course of the recorded oscillations combining large $\bar{g}_{Kir}$ values with low $\bar{g}_{Kleak}$ values (Fig. 7*B*, 34 nS and 0.3 nS, respectively). Indeed, we were able to generate both oscillations at frequencies below 0.2 Hz and large plateau potentials (Fig. 7*B*). Yet it was not possible to reproduce the exact shape of the plateaus by iteratively manipulating $\bar{g}_{Kir}$ and $\bar{g}_{Kleak}$. We then performed additional simulations including the cationic calcium-activated current I_{CAN}, which is known to mediate plateau potentials by producing an afterdepolarization that decays slowly because of its slow deactivation (Hughes et al. 2002; Zhu et al. 1999). Including I_{CAN} in the model (Fig. 7*C*, third trace) accurately and robustly reproduces the experimental traces for values of $\bar{g}_{Kir}$ and $\bar{g}_{Kleak}$ other than those underlying the S-NIC bifurcation ($\bar{g}_{Kir}$ = 30 nS and $\bar{g}_{Kleak}$ = 2.5 nS in Fig. 7*C* and data not shown). With this set of parameters (see Table 1), the modeled I_{Kir} (Fig. 7*C*, second trace) reproduces the time course of the dynamic-clamp injected current shown in Fig. 7*A* (second trace). The comparison with the time course of the gating variables of I_T (Fig. 7*C*, bottom trace) shows that the abrupt amplification of hyperpolarization induced by I_{Kir} removes nearly 100% of the inactivation of I_T (h_T increases). This hyperpolarization also induces the delayed activation of I_h (m_h). After that, I_{Kir} decreases as the membrane potential recovers toward the next LTS threshold, when the regenerative activation of I_T takes place (m_T^2).

DISCUSSION

All members of the inward rectifier potassium channel family Kir2, except the Kir2.6 subunit, are expressed in the central nervous system of rodents (Hibino et al. 2010; Karschin et al. 1996; Ryan et al. 2010). The main attributed role of these channels in the brain is regulation of cerebral blood flow by controlling microvascular tone and neurovascular coupling (Longden and Nelson 2015), which are mediated by nonneuronal Kir2 channels. Few studies have provided direct evidence for a role of Kir2.X channels on the intrinsic physiology of neurons (Amarillo et al. 2014; Carr and Surmeier 2007; Shen et al. 2007). In striatal cholinergic interneurons Kir2.X-like currents seem to play a prooscillatory function (Wilson 2005), whereas in neurons of the nociceptive pathway, in the dorsal spinal horn of neonate rats, Kir2 channels prevent the oscillations (Li et al. 2013). Here we used conductance-based models to demonstrate the theoretical basis for a pacemaker-promoting function of Kir2-like currents in TC neurons. To verify this prediction, we recorded rodent TC neurons in vitro and manipulated the levels of $\bar{g}_{Kir}$ with dynamic clamp.

We showed that the singular negative slope conductance region that characterizes the *I/V* curve of Kir2 channels generates bistability of the membrane potential when combined

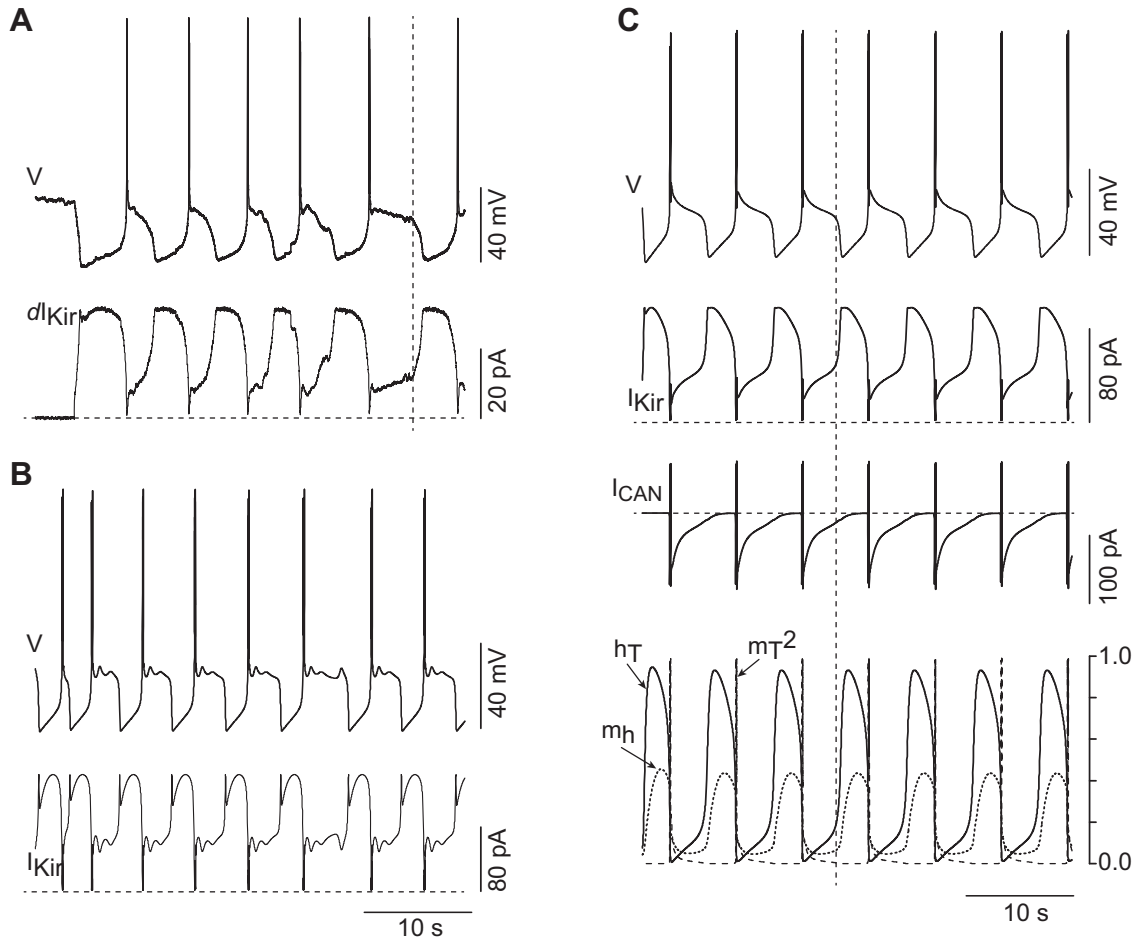

Fig. 7. Mechanism of dI_{Kir}-induced oscillations in TC neurons. *A*: membrane potential time course of repetitive bursts in a TC neuron (*top*) induced by introducing 10 nS d$\bar{g}_{Kirr}$. Time course of the current injected by the dynamic-clamp system is aligned (*bottom*). Regenerative activation of I_{Kir} (dashed vertical line) initiates the downstroke of a transient hyperpolarization. *B*: membrane potential (*top*) and I_{Kir} (*bottom*) time courses during repetitive bursts in a complete model of TC neuron using a large $\bar{g}_{Kir}$ value and a low $\bar{g}_{Kleak}$ value (34 nS and 0.3 nS, respectively) in the absence of I_{CAN}. See parameters for the other conductances in Table 1. *C*: simulations in the complete TC neuron model that includes the cationic calcium-activated current I_{CAN} (2.5 nS) using $\bar{g}_{Kir}$ = 30.6 nS and a more physiological $\bar{g}_{Kleak}$ value (2.5 nS). All parameters for these simulations are listed in Table 1. *Top*: time course of the membrane potential followed below by the time courses of I_{Kir} and I_{CAN}. *Bottom*: time course of the modeled activation of I_h (m_h, dotted trace) and the activation (m_T^2, dashed trace) and inactivation (h_T, solid trace) variables of I_T. Vertical dashed line is placed at an onset of regenerative activation of I_{Kir}, which coincides with an onset of activation of I_h and a large deinactivation of I_T. Horizontal dashed lines indicate the zero current level.

with leak conductances (Fig. 1). The linear, monotonic *I/V* relationship generated by the background leak conductances is transformed into a nonlinear, nonmonotonic *I/V* curve by effect of the Kir negative slope conductance, introducing instability in the membrane potential via saddle node bifurcations (Fig. 1). Note that the range at which this instability occurs coincides with the range of membrane potential at which physiological slow oscillations occur in TC neurons (see below). The dynamical properties of this one-dimensional system (formed by dV/dt) can be manipulated either by changing the injected current (as typically performed during electrophysiological experiments) or by changing the maximum potassium leak conductance (as occurs physiologically). Yet this is not sufficient to induce oscillations. Stable, robust oscillations are produced by the interaction between I_{Kir} and I_h in an I_{Kir}-I_h-Leaks model (Fig. 2). The *I/V* relationship of this minimal model increases monotonically as the membrane potential changes from negative to positive values, indicating that transitions between rest and oscillations (and vice versa) occur via Hopf bifurcations (Izhikevich 2005). Furthermore, these bifurcations are of the supercritical type, in which the resting state losses stability with the appearance of a stable limit cycle. To confirm further that the negative slope conductance region of I_{Kir} is the key feature of I_{Kir} that promotes periodicity, we performed bifurcation analysis using a modified Kir that lacks the negative slope conductance region of the I_{Kir}-I_h-Leaks and I_{Kir}-I_h-I_T-Leaks models (Fig. 4, *B* and *C*, respectively). Oscillations (limit cycle) are observed only when Kir has the negative slope conductance, whereas no oscillations are present when Kir lacks the negative slope.

In the I_{Kir}-Leaks model, bistability occurred via saddle node bifurcations when we used either $\bar{g}_{Kleak}$ (Fig. 1*C*) or current injection (Fig. 1, *A* and *B*) as the bifurcation parameter. When I_h is present, the model becomes a two-dimensional system formed by dV/dt and dm_h/dt, and different dynamical behaviors are obtained in response to either changes in $\bar{g}_{Kleak}$ or changes in current injection at hyperpolarized potentials. At these membrane potentials, changes in current injection in either direction (increase or decrease) produce a transition via a supercritical Hopf bifurcation (Fig. 2*C*). As the magnitude of

injected current decreases, the frequency of the oscillation suddenly drops to zero, imposing a lower limit of ~0.6 Hz (not illustrated). This supercritical Hopf bifurcation is equivalent to the supercritical Hopf bifurcation that occurs with values of $\bar{g}_{Kleak}$ of 1.1 nS (Fig. 2*D*). In contrast, for lower values of $\bar{g}_{Kleak}$, the stable limit cycle disappears via a saddle node on invariant circle bifurcation (S-NIC; Fig. 2*D*). This admits oscillations at very low frequencies (i.e., type I excitability), since the frequency decreases with the square root of $\bar{g}_{Kleak}$ (Fig. 2*D*, *inset*; see also Izhikevich 2005). This dynamical behavior is compatible with experimentally recorded oscillations in TC neurons at frequencies below 0.5 Hz (Figs. 5 and 7; see also Hughes et al. 2002).

To unveil the role of I_{Kir} in a model that also includes the oscillatory system provided by the activation and inactivation of I_T, we examined the bifurcation diagrams of the I_T-I_{Kir}-I_h-Leaks model in the presence or absence of I_{Kir}. We analyzed the effect of using the following bifurcation parameters: current injection (Fig. 3*A*), I_T maximum permeability (p_T, Fig. 3*B*), or $\bar{g}_{Kleak}$ (Fig. 3*C*). In the three cases, slow oscillations have larger amplitudes when I_{Kir} is present, and they also take place over an extended range of the bifurcation parameter. For example, the presence of $\bar{g}_{Kir}$ (9 nS) diminishes the requirement of I_T, since strong oscillations can now be produced with p_T as low as 10.7×10^{-9} cm^3/s (Fig. 3*B*). Furthermore, these oscillations occur under normal, physiological values of $\bar{g}_{Kleak}$ (2.7 nS). This indicates that the interaction between a large T current and/or a small leak conductance is not the only possible mechanism for intrinsic slow-wave sleep oscillations in TC neurons, as previously suggested (Crunelli et al. 2005). The dynamical behavior of the I_T-I_{Kir}-I_h-Leaks system in the presence of high Kir conductance and very low leak conductance further supports this notion. A high value of $\bar{g}_{Kir}$ (41 nS) gives rise to a S-NIC bifurcation (Fig. 3*D*), which endows the system with the ability to oscillate at frequencies below 0.5 Hz as the bifurcation point is approached at very low values of $\bar{g}_{Kleak}$ ($\approx$0.106 nS). These conditions also reproduce the time course of the oscillations observed experimentally (compare Fig. 3*D*, *inset*, with recording traces in Fig. 5 and Fig. 7).

Although the narrow conditions of high $\bar{g}_{Kir}$ and low $\bar{g}_{Kleak}$ used to model the dynamical behavior in Fig. 3*D* reproduce the time course of the oscillations observed experimentally, including the plateau potentials, adding the cationic calcium-dependent current I_{CAN} is required for the system to undergo slow oscillations and plateau potentials on a larger parameter space (see below). This setting would be more compatible with a highly variable, physiological scenario.

The results obtained with the reduced computational models of TC neurons predict that an increase in I_{Kir} induces robust slow oscillations of large amplitude in TC neurons. To test this experimentally, we recorded TC neurons from mouse brain slices and manipulated the amount of Kir conductance by dynamic clamp. In all TC neurons, the addition of certain magnitudes of I_{Kir} induces subthreshold oscillations at low frequencies, indicating that all the cells possess the necessary and sufficient ionic machinery that would interact with the added I_{Kir} to produce this periodic behavior. The range of minimal values of Kir conductance introduced by dynamic clamp for which we had obtained oscillations in the 19 mouse TC neurons tested was from 8 nS to 53 nS. Although the mean value (23.9 nS) was approximately three times larger than the mean value of endogenous Kir conductance (7.8 nS; range between 2.8 nS and 17.1 nS), the ranges of Kir conductance values are overlapping.

The oscillatory behavior of TC neurons depends on the balance of amplifying vs. resonant conductances (Amarillo et al. 2014; see also Marder et al. 2015). Hence, the wide range of Kir conductance values for which oscillations are obtained may reflect the existence of different levels of the other conductances in different cells, each requiring a certain value of Kir conductance to promote subthreshold oscillations. To test this directly, we induced oscillations in TC neurons from mice by increasing the availability of I_T (Fig. 6). Oscillations induced in this way disappear after pharmacological blockade of I_{Kir} and are rescued by addition of physiological magnitudes of $d\bar{g}_{Kir}$. This result strongly suggests that the intrinsic magnitude of $\bar{g}_{Kir}$ expressed by TC neurons from mice has a promoting effect on slow periodicity.

In Fig. 7 we provide a mechanistic explanation for the oscillations induced by adding artificial I_{Kir} to TC neurons from mice. Regenerative activation (unblock) of I_{Kir} amplifies hyperpolarization (Fig. 7, *A* and *C*); this powerful hyperpolarization strongly activates resonant I_h (Fig. *7C*, *bottom*) and almost totally removes inactivation of I_T (h_T approaches 1.0; Fig. 7*C*, *bottom*); the slow activation of I_h brings the membrane potential toward the point of regenerative activation of highly available I_T; regenerative activation of I_T produces the upstroke of the LTS; and the subsequent inactivation of this current produces the repolarization of the membrane potential after the burst of Na^+/K^+-mediated action potentials. This repolarization brings the membrane potential to the point where regenerative activation of I_{Kir} reinitiates the cycle.

Besides the inactivation of I_T, several ionic conductances participate in the repolarization of the membrane potential during the downstroke of the LTS (Amarillo et al. 2014; Hughes et al. 2002; McCormick and Huguenard 1992; Zhu et al. 1999). In particular, the cationic calcium-dependent current I_{CAN} is activated during the LTS, producing a slowly decaying afterdepolarization. The kinetics of this depolarization depends on the slow time constant of deactivation of I_{CAN} (third trace in Fig. 7*C*; Hughes et al. 2002; Zhu et al. 1999). Without I_{CAN} in our simulations, it was possible to generate oscillations that resemble the recorded behavior (very low frequencies and plateaus) only if we used a very specific set of Kir and Kleak parameters (Fig. 7*B*). Plateaus are generated in this case by the balance between the weak hyperpolarizing drive provided by a small I_{Kleak} and all the depolarizing conductances that are active at the end of the LTS (i.e., I_{Naleak}, steady state-activated I_{NaP} and I_h, and the window current component of I_T; Amarillo et al. 2014). In this scenario, regenerative activation of I_{Kir} is triggered by membrane potential fluctuations that reach a not-returning point (see membrane potential fluctuations following LTSs in Fig. 7*B*). Including I_{CAN} in the model reproduces—for a more physiological range of I_{Kleak} magnitudes—the slow frequency of the oscillations and the shape of the time course of the membrane potential, especially the decaying plateaus. The depolarizing drive of activated I_{CAN} counteracts I_{Kleak}-mediated hyperpolarization, forcing the membrane potential to follow its slow deactivation kinetics. In this last scenario, regenerative activation of I_{Kir} is reached smoothly at a point where I_{CAN} is sufficiently deactivated (Fig. 7, *A* and *C*).

It has been proposed that the bistability that underlies intrinsic slow oscillations in TC neurons is generated by the interaction of the window current component of I_T and the leak current (Crunelli et al. 2005; Hughes et al. 1999, 2002). According to this model, the magnitudes of these two currents have to be balanced in such a way that the *I/V* relationship of the system becomes nonmonotonic. When this happens, oscillations result from the alternating destabilization of two stable equilibria: one is destabilized by deactivation of I_{CAN} at depolarized potentials, followed by the destabilization of the other by activation of I_h at hyperpolarized potentials (Crunelli et al. 2005; Hughes et al. 1999). Here we proposed an alternative scenario in which the dynamical interaction between the voltage- and time-dependent properties of I_{Kir} (fast-amplifying current) and I_h (slow resonant current) generates slow oscillations even though the total steady-state *I/V* curve is monotonic. This slow system interacts with the intrinsically oscillatory system formed by the activation and inactivation gates of I_T, increasing the robustness of the oscillation.

Delta and slow brain rhythms (<4 Hz) have been linked to changes in synaptic strength and structural remodeling of dendritic spines, which are believed to be the basis of memory consolidation (Wei et al. 2016; Yang et al. 2014). TC neurons seem to play a critical role in the generation and maintenance of these globally synchronized low-frequency oscillations, which are characteristic of unconscious states like deep stages of NREM sleep (Steriade 1997) and absence seizures (Steriade and Contreras 1995). The pacemaker activity of TC neurons could be controlled by modulating the balance among the different ion conductances (through interaction with synaptic inputs and network dynamics) to generate the diversity of membrane potential oscillations observed at different behavioral states. For this reason, great attention has been placed on studying modulatory mechanisms of I_{Kleak}, I_h, and I_T in these neurons (Cheong et al. 2008; Leresche et al. 2004; McCormick 1992; McCormick and Pape 1990a; Yue and Huguenard 2001; Zhu and Uhlrich 1998). Our results suggest that the strong inward rectifier potassium current I_{Kir} should be added to this list, given its prooscillatory role in TC neurons demonstrated here. Several signaling cascades, including the phosphatidylinositol 4,5-bisphosphate pathway via lipid kinases and the PKA and src kinase pathways, are known to regulate the activity of Kir2.2 channels (reviewed in Hibino et al. 2010). These and other undiscovered Kir2.2 modulatory mechanisms could probe important in the regulation of the pacemaker propensity of TC neurons and hence in the regulation of the slow brain rhythms. In addition to these physiological modulations, gain-of-function mutations in Kir channels expressed in the heart have been shown to underlie diseases such as atrial fibrillation (Li et al. 2004; Xia et al. 2005). Similar gain-of-function mutations in the Kir2.2 channels expressed by TC neurons might explain the putative increase in Kir conductance that could induce pathological spike and wave oscillations during absence seizures, a hypothesis that stems from our present study.

Finally, the overexpression of strong inward rectifier potassium channels of the Kir2 family (see, for example, Nitabach et al. 2002; Yoon et al. 2008) is a commonly used technique for silencing a particular population of neurons. Here we demonstrate that the negative slope conductance region in the *I/V* curve of these channels amplifies the hyperpolarization and promotes oscillations when combined with resonant I_h. Therefore, caution must be taken when using this technique, since overexpression of Kir channels in cells that express I_h could result in a "paradoxical" increase of excitability.

GRANTS

This work was subsidized by Consejo Nacional de Investigaciones Científicas y Técnicas-Argentina PIP 0256 and a doctoral fellowship to A. I. Tissone.

DISCLOSURES

No conflicts of interest, financial or otherwise, are declared by the authors.

AUTHOR CONTRIBUTIONS

Y.A. and M.S.N. conceived and designed research; Y.A. performed experiments; Y.A., A.I.T., G.M., and M.S.N. analyzed data; Y.A., A.I.T., G.M., and M.S.N. interpreted results of experiments; Y.A. and M.S.N. prepared figures; Y.A., G.M., and M.S.N. drafted manuscript; Y.A., A.I.T., G.M., and M.S.N. edited and revised manuscript; Y.A., A.I.T., G.M., and M.S.N. approved final version of manuscript.

REFERENCES

Amarillo Y, De Santiago-Castillo JA, Dougherty K, Maffie J, Kwon E, Covarrubias M, Rudy B. Ternary Kv4.2 channels recapitulate voltage-dependent inactivation kinetics of A-type K^+ channels in cerebellar granule neurons. *J Physiol* 586: 2093–2106, 2008. doi:10.1113/jphysiol.2007.150540.

Amarillo Y, Mato G, Nadal MS. Analysis of the role of the low threshold currents IT and Ih in intrinsic delta oscillations of thalamocortical neurons. *Front Comput Neurosci* 9: 52, 2015. doi:10.3389/fncom.2015.00052.

Amarillo Y, Zagha E, Mato G, Rudy B, Nadal MS. The interplay of seven subthreshold conductances controls the resting membrane potential and the oscillatory behavior of thalamocortical neurons. *J Neurophysiol* 112: 393–410, 2014. doi:10.1152/jn.00647.2013.

Anumonwo JM, Lopatin AN. Cardiac strong inward rectifier potassium channels. *J Mol Cell Cardiol* 48: 45–54, 2010. doi:10.1016/j.yjmcc.2009.08.013.

Buzsáki G. *Rhythms of the Brain*. New York: Oxford Univ. Press, 2006, p. 175–205. doi:10.1093/acprof:oso/9780195301069.001.0001.

Carr DB, Surmeier DJ. M1 muscarinic receptor modulation of Kir2 channels enhances temporal summation of excitatory synaptic potentials in prefrontal cortex pyramidal neurons. *J Neurophysiol* 97: 3432–3438, 2007. doi:10.1152/jn.00828.2006.

Cheong E, Lee S, Choi BJ, Sun M, Lee CJ, Shin HS. Tuning thalamic firing modes via simultaneous modulation of T- and L-type Ca^{2+} channels controls pain sensory gating in the thalamus. *J Neurosci* 28: 13331–13340, 2008. doi:10.1523/JNEUROSCI.3013-08.2008.

Crunelli V, Tóth TI, Cope DW, Blethyn K, Hughes SW. The "window" T-type calcium current in brain dynamics of different behavioural states. *J Physiol* 562: 121–129, 2005. doi:10.1113/jphysiol.2004.076273.

Curró-Dossi R, Nuñez A, Steriade M. Electrophysiology of a slow (0.5-4 Hz) intrinsic oscillation of cat thalamocortical neurones in vivo. *J Physiol* 447: 215–234, 1992. doi:10.1113/jphysiol.1992.sp018999.

Dhamoon AS, Pandit SV, Sarmast F, Parisian KR, Guha P, Li Y, Bagwe S, Taffet SM, Anumonwo JM. Unique Kir2.x properties determine regional and species differences in the cardiac inward rectifier K^+ current. *Circ Res* 94: 1332–1339, 2004. doi:10.1161/01.RES.0000128408.66946.67.

Dreyfus FM, Tscherter A, Errington AC, Renger JJ, Shin HS, Uebele VN, Crunelli V, Lambert RC, Leresche N. Selective T-type calcium channel block in thalamic neurons reveals channel redundancy and physiological impact of $I_{Twindow}$. *J Neurosci* 30: 99–109, 2010. doi:10.1523/JNEUROSCI.4305-09.2010.

Ermentrout B. *Simulating, Analyzing, and Animating Dynamical Systems: A Guide to Xppaut for Researchers and Students*. Philadelphia, PA: SIAM, 2002. doi:10.1137/1.9780898718195.

Ernst WL, Zhang Y, Yoo JW, Ernst SJ, Noebels JL. Genetic enhancement of thalamocortical network activity by elevating alpha1G-mediated low-voltage-activated calcium current induces pure absence epilepsy. *J Neurosci* 29: 1615–1625, 2009. doi:10.1523/JNEUROSCI.2081-08.2009.

Hibino H, Inanobe A, Furutani K, Murakami S, Findlay I, Kurachi Y. Inwardly rectifying potassium channels: their structure, function, and physiological roles. *Physiol Rev* 90: 291–366, 2010. doi:10.1152/physrev.00021.2009.

Hille B. *Ionic Channels of Excitable Membranes*. Sunderland, MA: Sinauer, 2001.

Hines ML, Carnevale NT. The NEURON simulation environment. *Neural Comput* 9: 1179–1209, 1997. doi:10.1162/neco.1997.9.6.1179.

Huguenard JR, Coulter DA, Prince DA. A fast transient potassium current in thalamic relay neurons: kinetics of activation and inactivation. *J Neurophysiol* 66: 1304–1315, 1991. doi:10.1152/jn.1991.66.4.1304.

Hughes SW, Cope DW, Blethyn KL, Crunelli V. Cellular mechanisms of the slow (<1 Hz) oscillation in thalamocortical neurons in vitro. *Neuron* 33: 947–958, 2002. doi:10.1016/S0896-6273(02)00623-2.

Hughes SW, Cope DW, Tóth TI, Williams SR, Crunelli V. All thalamocortical neurones possess a T-type Ca^{2+} "window" current that enables the expression of bistability-mediated activities. *J Physiol* 517: 805–815, 1999. doi:10.1111/j.1469-7793.1999.0805s.x.

Hughes SW, Lorincz M, Cope DW, Crunelli V. Using the dynamic clamp to dissect the properties and mechanisms of intrinsic thalamic oscillations. In: *Dynamic-Clamp From Principles to Applications*, edited by Destexhe A, Bal T. New York: Springer, 2009, p. 321–346.

Hutcheon B, Yarom Y. Resonance, oscillation and the intrinsic frequency preferences of neurons. *Trends Neurosci* 23: 216–222, 2000. doi:10.1016/S0166-2236(00)01547-2.

Izhikevich E. *Dynamical Systems in Neuroscience: The Geometry of Excitability and Bursting*. Cambridge, MA: MIT Press, 2005.

Jacobsen RB, Ulrich D, Huguenard JR. $GABA_B$ and NMDA receptors contribute to spindle-like oscillations in rat thalamus in vitro. *J Neurophysiol* 86: 1365–1375, 2001. doi:10.1152/jn.2001.86.3.1365.

Karschin C, Dissmann E, Stühmer W, Karschin A. IRK(1-3) and GIRK(1-4) inwardly rectifying K^+ channel mRNAs are differentially expressed in the adult rat brain. *J Neurosci* 16: 3559–3570, 1996. doi:10.1523/JNEUROSCI.16-11-03559.1996.

Kemenes I, Marra V, Crossley M, Samu D, Staras K, Kemenes G, Nowotny T. Dynamic clamp with StdpC software. *Nat Protoc* 6: 405–417, 2011. doi:10.1038/nprot.2010.200.

Kim D, Song I, Keum S, Lee T, Jeong MJ, Kim SS, McEnery MW, Shin HS. Lack of the burst firing of thalamocortical relay neurons and resistance to absence seizures in mice lacking $alpha_{1G}$ T-type Ca^{2+} channels. *Neuron* 31: 35–45, 2001. doi:10.1016/S0896-6273(01)00343-9.

Lee J, Kim D, Shin HS. Lack of delta waves and sleep disturbances during non-rapid eye movement sleep in mice lacking alpha1G-subunit of T-type calcium channels. *Proc Natl Acad Sci USA* 101: 18195–18199, 2004. doi:10.1073/pnas.0408089101.

Leresche N, Hering J, Lambert RC. Paradoxical potentiation of neuronal T-type Ca^{2+} current by ATP at resting membrane potential. *J Neurosci* 24: 5592–5602, 2004. doi:10.1523/JNEUROSCI.1038-04.2004.

Leresche N, Lightowler S, Soltesz I, Jassik-Gerschenfeld D, Crunelli V. Low-frequency oscillatory activities intrinsic to rat and cat thalamocortical cells. *J Physiol* 441: 155–174, 1991. doi:10.1113/jphysiol.1991.sp018744.

Li J, Blankenship ML, Baccei ML. Inward-rectifying potassium (Kir) channels regulate pacemaker activity in spinal nociceptive circuits during early life. *J Neurosci* 33: 3352–3362, 2013. doi:10.1523/JNEUROSCI.4365-12.2013.

Li J, McLerie M, Lopatin AN. Transgenic upregulation of I_{K1} in the mouse heart leads to multiple abnormalities of cardiac excitability. *Am J Physiol Heart Circ Physiol* 287: H2790–H2802, 2004. doi:10.1152/ajpheart.00114.2004.

Llinás R, Jahnsen H. Electrophysiology of mammalian thalamic neurones in vitro. *Nature* 297: 406–408, 1982. [Erratum in *Nature* 298: 496, 1982.] doi:10.1038/297406a0.

Longden TA, Nelson MT. Vascular inward rectifier K^+ channels as external K^+ sensors in the control of cerebral blood flow. *Microcirculation* 22: 183–196, 2015. doi:10.1111/micc.12190.

Ludwig A, Budde T, Stieber J, Moosmang S, Wahl C, Holthoff K, Langebartels A, Wotjak C, Munsch T, Zong X, Feil S, Feil R, Lancel M, Chien KR, Konnerth A, Pape HC, Biel M, Hofmann F. Absence epilepsy and sinus dysrhythmia in mice lacking the pacemaker channel HCN2. *EMBO J* 22: 216–224, 2003. doi:10.1093/emboj/cdg032.

Marder E, Goeritz ML, Otopalik AG. Robust circuit rhythms in small circuits arise from variable circuit components and mechanisms. *Curr Opin Neurobiol* 31: 156–163, 2015. doi:10.1016/j.conb.2014.10.012.

McCormick DA. Cellular mechanisms underlying cholinergic and noradrenergic modulation of neuronal firing mode in the cat and guinea pig dorsal lateral geniculate nucleus. *J Neurosci* 12: 278–289, 1992. doi:10.1523/JNEUROSCI.12-01-00278.1992.

McCormick DA, Huguenard JR. A model of the electrophysiological properties of thalamocortical relay neurons. *J Neurophysiol* 68: 1384–1400, 1992. doi:10.1152/jn.1992.68.4.1384.

McCormick DA, Pape HC. Noradrenergic and serotonergic modulation of a hyperpolarization-activated cation current in thalamic relay neurones. *J Physiol* 431: 319–342, 1990a. doi:10.1113/jphysiol.1990.sp018332.

McCormick DA, Pape HC. Properties of a hyperpolarization-activated cation current and its role in rhythmic oscillation in thalamic relay neurones. *J Physiol* 431: 291–318, 1990b. doi:10.1113/jphysiol.1990.sp018331.

McCormick DA, Prince DA. Actions of acetylcholine in the guinea-pig and cat medial and lateral geniculate nuclei, in vitro. *J Physiol* 392: 147–165, 1987. doi:10.1113/jphysiol.1987.sp016774.

McCormick DA, Prince DA. Noradrenergic modulation of firing pattern in guinea pig and cat thalamic neurons, in vitro. *J Neurophysiol* 59: 978–996, 1988. doi:10.1152/jn.1988.59.3.978.

Meuth SG, Kanyshkova T, Meuth P, Landgraf P, Munsch T, Ludwig A, Hofmann F, Pape HC, Budde T. Membrane resting potential of thalamocortical relay neurons is shaped by the interaction among TASK3 and HCN2 channels. *J Neurophysiol* 96: 1517–1529, 2006. doi:10.1152/jn.01212.2005.

Nitabach MN, Blau J, Holmes TC. Electrical silencing of *Drosophila* pacemaker neurons stops the free-running circadian clock. *Cell* 109: 485–495, 2002. doi:10.1016/S0092-8674(02)00737-7.

Rush ME, Rinzel J. Analysis of bursting in a thalamic neuron model. *Biol Cybern* 71: 281–291, 1994. doi:10.1007/BF00239616.

Ryan DP, Dias da Silva MR, Soong TW, Fontaine B, Donaldson MR, Kung AW, Jongjaroenprasert W, Liang MC, Khoo DH, Cheah JS, Ho SC, Bernstein HS, Maciel RM, Brown RH Jr, Ptácek LJ. Mutations in potassium channel Kir2.6 cause susceptibility to thyrotoxic hypokalemic periodic paralysis. *Cell* 140: 88–98, 2010. doi:10.1016/j.cell.2009.12.024.

Schram G, Pourrier M, Wang Z, White M, Nattel S. Barium block of Kir2 and human cardiac inward rectifier currents: evidence for subunit-heteromeric contribution to native currents. *Cardiovasc Res* 59: 328–338, 2003. doi:10.1016/S0008-6363(03)00366-3.

Shen W, Tian X, Day M, Ulrich S, Tkatch T, Nathanson NM, Surmeier DJ. Cholinergic modulation of Kir2 channels selectively elevates dendritic excitability in striatopallidal neurons. *Nat Neurosci* 10: 1458–1466, 2007. doi:10.1038/nn1972.

Soltesz I, Lightowler S, Leresche N, Jassik-Gerschenfeld D, Pollard CE, Crunelli V. Two inward currents and the transformation of low-frequency oscillations of rat and cat thalamocortical cells. *J Physiol* 441: 175–197, 1991. doi:10.1113/jphysiol.1991.sp018745.

Steriade M. Synchronized activities of coupled oscillators in the cerebral cortex and thalamus at different levels of vigilance. *Cereb Cortex* 7: 583–604, 1997. [Erratum in *Cereb Cortex* 7: 779, 1997.] doi:10.1093/cercor/7.6.583.

Steriade M, Contreras D. Relations between cortical and thalamic cellular events during transition from sleep patterns to paroxysmal activity. *J Neurosci* 15: 623–642, 1995. doi:10.1523/JNEUROSCI.15-01-00623.1995.

Steriade M, Contreras D, Amzica F, Timofeev I. Synchronization of fast (30–40 Hz) spontaneous oscillations in intrathalamic and thalamocortical networks. *J Neurosci* 16: 2788–2808, 1996. doi:10.1523/JNEUROSCI.16-08-02788.1996.

Warren RA, Agmon A, Jones EG. Oscillatory synaptic interactions between ventroposterior and reticular neurons in mouse thalamus in vitro. *J Neurophysiol* 72: 1993–2003, 1994. doi:10.1152/jn.1994.72.4.1993.

Wei Y, Krishnan GP, Bazhenov M. Synaptic mechanisms of memory consolidation during sleep slow oscillations. *J Neurosci* 36: 4231–4247, 2016. doi:10.1523/JNEUROSCI.3648-15.2016.

Wilson CJ. The mechanism of intrinsic amplification of hyperpolarizations and spontaneous bursting in striatal cholinergic interneurons. *Neuron* 45: 575–585, 2005. doi:10.1016/j.neuron.2004.12.053.

Xia M, Jin Q, Bendahhou S, He Y, Larroque MM, Chen Y, Zhou Q, Yang Y, Liu Y, Liu B, Zhu Q, Zhou Y, Lin J, Liang B, Li L, Dong X, Pan Z, Wang R, Wan H, Qiu W, Xu W, Eurlings P, Barhanin J, Chen Y. A Kir2.1 gain-of-function mutation underlies familial atrial fibrillation. *Biochem Biophys Res Commun* 332: 1012–1019, 2005. doi:10.1016/j.bbrc.2005.05.054.

Yang G, Lai CS, Cichon J, Ma L, Li W, Gan WB. Sleep promotes branch-specific formation of dendritic spines after learning. *Science* 344: 1173–1178, 2014. doi:10.1126/science.1249098.

Yoon YJ, Kominami H, Trimarchi T, Martin-Caraballo M. Inhibition of electrical activity by retroviral infection with Kir2.1 transgenes disrupts electrical differentiation of motoneurons. *PLoS One* 3: e2971, 2008. doi:10.1371/journal.pone.0002971.

Yue BW, Huguenard JR. The role of H-current in regulating strength and frequency of thalamic network oscillations. *Thalamus Relat Syst* 1: 95–103, 2001. doi:10.1017/S1472928801000097.

Zhu JJ, Uhlrich DJ. Cellular mechanisms underlying two muscarinic receptor-mediated depolarizing responses in relay cells of the rat lateral geniculate nucleus. *Neuroscience* 87: 767–781, 1998. doi:10.1016/S0306-4522(98)00209-7.

Zhu JJ, Uhlrich DJ, Lytton WW. Burst firing in identified rat geniculate interneurons. *Neuroscience* 91: 1445–1460, 1999. doi:10.1016/S0306-4522(98)00665-4.